Role of Dynein Light Chains Tctex1 and Tcte3 in Apoptosis through *In-silico* Approaches

By

Sonia Kanwal

National Centre for Bioinformatics

Faculty of Biological Sciences

Quaid-i-Azam University Islamabad, Pakistan

2017

Role of Dynein Light Chains Tctex1 and Tcte3 in Apoptosis through *In-silico* Approaches

A Thesis submitted in the partial fulfillment of the requirements for the degree of

Master of Philosophy in Bioinformatics

By

Sonia Kanwal

Supervisor

Dr. Sajid Rashid

National Center for Bioinformatics

Faculty of Biological Sciences

Quaid-i-Azam University, Islamabad, Pakistan

2017

Dedicated

To

MY AFFECTIONATE AND LOVING

Beloved Parents and Siblings

CERTIFICATE

This thesis is submitted by **Sonia Kanwal** from National Center for Bioinformatics, Faculty of Biological Sciences, Quaid-i-Azam University, Islamabad, Pakistan, is accepted in its present form as satisfying the thesis requirements for the Degree of Master of Philosophy in Bioinformatics.

Internal Examiner: _____

Dr. Sajid Rashid

Associate Professor & Supervisor

Quaid-i-Azam University, Islamabad

External Examiner: _____

Dr. XYZ

Designation

Corresponding Institutional Address

Chairperson: _____

Dr. Sajid Rashid

Associate Professor

Quaid-i-Azam University, Islamabad

Date: 21 July, 2017

DECLARATION

I hereby solemnly declare that the work **"Role of Dynein Light Chains Tctex1 and Tcte3 in Apoptosis through *In-silico* Approaches"** presented in the following thesis is my own effort, except where otherwise acknowledged and the thesis is my own composition. No part of the thesis has been previously presented for any other degree.

Dated: _____ _____

Sonia Kanwal

Abstract

Cytoplasmic dynein is a main motor protein that is accountable for microtubule minus-end-directed activities in the eukaryotic cells. It transports a large range of cargoes and exhibits frequent functions during spindle congregation and chromosome separation. Dynein light chains (Tctex1 and Tcte3) add diversity in dynein function by connecting specific cargoes to the dynein complex. Tctex1 and Tcte3 are germ cell specific proteins with higher expression levels in testis and play a vital role in male germ cell development. Dynein complex plays an important role in the regulation of apoptosis by carrying pro- and anti-apoptotic cargoes. In this study, we investigated the role of Tctex1 and Tcte3 in apoptosis by computational approaches. We modeled Tctex1, Tcte3 tertiary structures to explore their structural similarities with dynein light chain of 8 kDa (LC8) which is experimentally known dynein light chain having role in apoptosis. Multiple docking procedures were employed to validate homodimerization and binding groove for pro-apoptotic protein Bim. Molecular dynamics simulation analysis was performed to confirm the stability and residual flexibility of apo-Tctex1,Tcte3 and their complexes with Bim. The simulation analysis demonstrated an overall stable binding pattern. We propose that like LC8, Tctex1 and Tcte3 exhibit similar dimer topology and binding grooves for Bim. Due to structural similarity, common binding partners, identical binding pocket and functional relevance, Tctex1 and Tcte3 may have common roles in apoptotic pathway by interacting with Bim in a similar manner to that of LC8.

Acknowledgements

All praise to Almighty **ALLAH** for giving me the strength to complete this piece of research work. My humble gratitude for **Holy Prophet (S.A.W.W.)**, for his guidance towards the righteous path and for his teachings especially about seeking knowledge and spreading it.

First and foremost, I would like to express my gratitude to my Supervisor, **Dr. Sajid Rashid** for his keen supervision throughout the project, for the time he spent from laying the foundation of the project till its extension and completion, for his insightful comments and for providing all the resources required for this project. I am also obliged for his patience and tolerance.

I am deeply thankful to **Prof. Dr. Zabta Khan Shinwari**, Dean of Biological Sciences and my sincere gratitude to Chairman of National Center for Bioinformatics **Dr. Sajid Rashid** for their commendable role in providing congenial environment and research facilities which made my research work possible.

All of my esteemed teachers, throughout my educational career have been an inspiration for me, all in their own way. I would like to acknowledge all my teachers, whose knowledge and training helped me to learn valuable lessons not just for the sake of education but for life.

I owe a special thanks to all the members of the *Functional Informatics lab*, especially to**, Shagufta Shafique, Saima Younas, Muhammad Fakhar, Maryam Rozi, Imran sharif, Mehreen Jan, Waqar Ali, Faiza Siddique, Shumaila Khan, Wajahat Khan and Tehreem Ashraf** with whom I interacted during my research. They maintained friendly and cheerful environment during whole period of my stay in lab and I really admire how they inculcate enthusiasm in each other.

Finally, I must express my very profound gratitude to my caring friends **Zunera Khalid, Neenish Rana and Nosheen Ehsan** for providing me with unfailing support and continuous encouragement throughout my years of study and through the process

of researching and writing this thesis. This accomplishment would not have been possible without them.

At this Juncture, I thank of my parents **Mr. and Mrs. Syed Abrar Hussain Shah and my Uncle Syed Sheraz** whose selfless sacrificial life and their great efforts and unceasing prayers have enabled me to reach the present position in life. My deepest gratitude goes to my family for their unflagging love support throughout my life, this research report is simply impossible without them. My thanks are tendered to my loving, caring, and sincere parents, sister and brothers **Syed Shahid Hussain Shah** and **Syed Sharjeel Hassan Shah** and family members for their ever-lasting cooperation and prayers.

Syeda Sonia

Table of Contents

List of Abbreviations

Hc	Heavy chain
Ic	Intermediate chain
ILc	Intermediate Light chain
Lc	Light chain
AAA	ATPases related with Assorted Action
kDa	Kilo Daltons
DYNC1H1	Dynein Heavy Chain
DYNC1I1	Dynein Intermediate chain
DYNC1LI1	Dynein Light Intermediate Chain
DYNLT1	Dynein Light Chain
DICs	Dynein Intermediate Chains
UniProtKB	UniProtKnowledgeBase
PDB	Protein Data Bank
RCSB	Research Collaboratory for Structural Bioinformatics
UCSF	University of California, San Francisco
LGA	Lamarckian Genetic Algorithm
GROMACS	Groningen Machine for Chemical simulation
RMSD	Root Mean Square Deviation
RMSF	Root Mean Square Fluctuation
NPT	Number of particles, Pressure, Temperature
NVT	Number of particles, Volume, Temperature
MD simulation	Molecular Dynamics simulation
3D	3-Dimensional
PSI-BLAST	Position-Specific-Iterative BLAST
BLAST	Basic Local Alignment Search Tool
CPORT	Consensus Prediction Of Interface Residues in Transient complexes
FFT	Fast Fourier Transform
SDU	Semi-Definite programming based Underestimation

PBC	Periodic Boundary Condition
PME	Particle Mesh Ewald
E-value	Expected-value
AMBER	Assisted Model Building with Energy Refinement
NMR	Nuclear Magnetic Resonance spectroscopy
MEFs	Mouse Embryonic Fibroblasts
BAX	BCL2-Associated X
BAK	BCL2-Antagonists/Killer
Pak1	p21-activated Kinase-1
MAPK8	Mitogen-Activated Protein Kinase-8
JNK	Jun N-terminal Kinase

Three and one letter code of twenty amino acids

Amino acids	**Three letter codes**	**One letter codes**
Alanine	Ala	A
Arginine	Arg	R
Asparagine	Asn	N
Aspartate	Asp	D
Cystine	Cys	C
Lysine	Lys	K
Glutamate	Glu	E
Glycine	Gly	G
Glutamine	Gln	Q
Histidine	His	H
Isoleucine	Ile	I
Leucine	Leu	L
Methionin	Met	M
Phenylalanine	Phe	F
Proline	Pro	P
Serine	Ser	S

Tyrosine	Tyr	Y
Valine	Val	V
Threonine	Thr	T
Tryptophan	Trp	W

List of Figures

List of Tables

1. INTRODUCTION

1.1 Motor proteins

Motor proteins act as molecular machines that are capable of cell motility by utilizing energy derived through ATP hydrolysis. In cytoplasm, cellular cargos and vesicles are transported by driving force of motor proteins. Several motor proteins (kinesin and cytoplasmic dynein) play important role in intracellular transport (axonal transport), spindle apparatus formation and chromosomes separation during cell division process (Gittes *et al.*, 1993).

1.2 Cytoskeletal motor proteins

The movement of motor proteins is carried out in two ways on the basis of their substrates. Actin motors (myosin) follow the movement along microfilaments by considering actin interaction. Microtubule motors (kinesin and dynein) move with the help of microtubules through tubulin interaction. Cytoskeletal motor proteins are classified into two categories based on carrying movement direction along microtubules within cell i.e., plus-end motors: actin motors and minus-end motors: microtubule motors (Baas and Ahmad, 2001).

There are prominent similarities in these three cytoskeletal motors (myosin, kinesin, and dynein) as they are independently evolved and not homologues. Each motor protein converts chemical energy into mechanical energy by means of ATP hydrolysis **(**Gittes *et al.*,1993). All motor proteins exist in complex form which consists of several components. The regulation of motor activity is mediated by heavy chain. The intermediate and light chains arbitrate the tethering of motor to molecular cargo. The heavy chain is structured into two domains. The head (globular) domain incorporates the ATP-sensitive track-interacting region and the ATP hydrolysis. The tail (extended) domain is responsible for linking motor to cargo by interacting with other subunits (Asai and Wilkes, 2004).

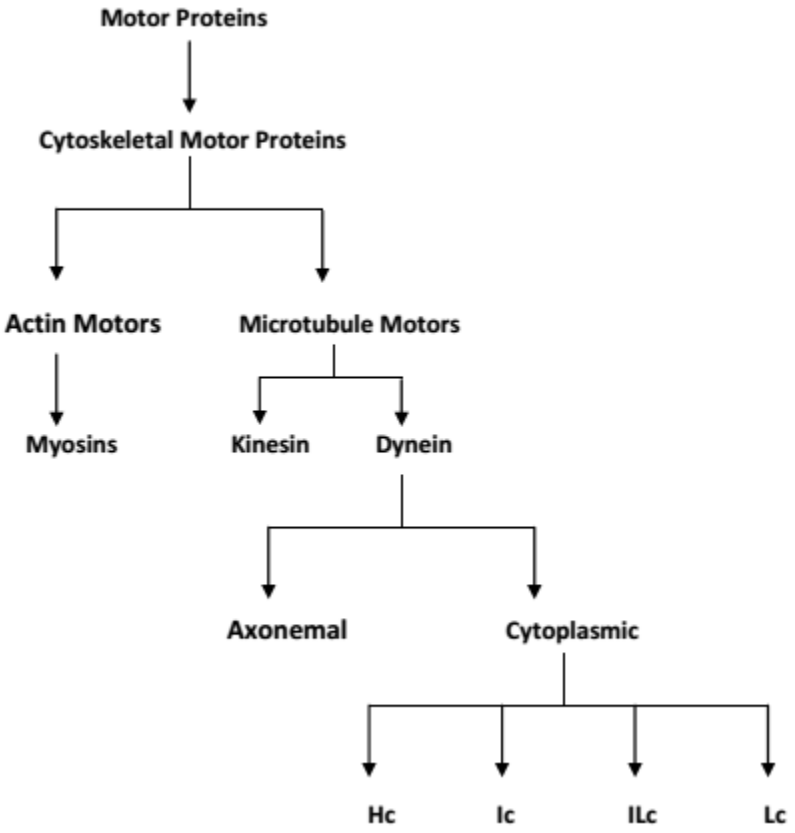

Figure 1.1: Classification of motor proteins. Motor proteins are represented in flow chart. There are total five levels: at '0' level motor proteins, '1' level shows example of motor proteins and '2' represents the categories of Cytoskeletal motor proteins (actin and microtubule). At '3' level examples of microtubule (kinesin, dynein) and actin motors (myosins) are represented . Level '4' illustrates the classification of dyneins into two categories (axonemal and cytoplasmic). For further classification of cytoplasmic dyneins level '5' describes the four chains (Heavy chain: Hc, Intermediate chain: Ic, Intermediate Light chain: ILc and Light chain: Lc).

1.2.1 Actin motors

Actin motors are connected in a manner to form hetero-motor complexes. The best example of such confirmation is ‘myosin’ (Goode *et al.*, 2000).

1.2.2 Myosin

Muscle contraction is generated by primary recognized myosin (myosin II). Myosin II protein is composed of two heavy chains (motor head) and two light chains. Myosin head contains ATP and actin interaction sites. The movement towards plus (+) end of actin filament provides energy. In cell division, myosin II plays an essential role. Bipolar thick filaments of myosin II divide parent cell into two daughter cells by contraction force during cytokinesis. Myosin is also responsible for multiple non-muscle cells movement. At cell surface, myosin I is engaged in intracellular association and the projection of structures (actin-rich). Organelle and vesicle transport is proscribed by myosin V (Alberts, 2002). Myosin XI is involved in the cytoplasmic streaming which allows organelles to stream along with microfilaments (Thompson and Langford, 2002).

1.2.3 Microtubule motors

In essential cellular functions (vesicle trafficking and cell division), motor proteins utilize microtubules as substrates. Microtubules are involved in interaction with major motor proteins like kinesin (moves towards microtubule positive end) and dynein (moves towards negative end of microtubule) (Hirokawa *et al.,* 2009).

1.2.3.1 Kinesin

Kinesin generates the motile strength by driving conformational changes through the utilization of ATP hydrolysis (Hirokawa and Noda, 2008). Kinesin is a superfamily proteins, act as significant motor proteins for transportation of cargos. Kinesin is involved in the transportation of protein complexes, mRNAs and membrane bounded organelles. Recent studies suggest different mechanisms to recognize kinesin binding to specific cargos, unloading and adjusting the direction of movement. Recent *in- vivo* experiments have exposed imperative and unpredicted functions of kinesins in various physiological processes (developmental patterning, brain function and tumor repression) (Hirokawa *et al.,* 2009).

1.2.3.2 Dynein

Dynein is one of the cytoskeletal motor proteins that is essential for smooth movement of microtubules through the thrashing of cilia and flagella located on eukaryotic cell surfaces (Roberts *et al.,* 2013). Dynein belongs to superfamily AAA (ATPases related with assorted actions) (Neuwald *et al.,* 1999). Dyneins are divided into two groups: axonemal and cytoplasmic dyneins.

1.2.3.2.1 Axonemal dynein

Axonemal dyneins exist in complex form by containing one, two or three non-identical heavy chains depending on organism and cilium location. Heavy chain is comprised of doughnut-shaped structure (globular motor domain) similar to AAA proteins, a twisting coil 'stalk' (interacts with microtubule), and an elongated tail (stem) which binds to adjacent microtubule of similar axoneme. The regulated activity of axonemal dynein is significant for ciliary waveform and flagellar strike frequency. The regulation of axonemal dynein includes calcium mode, phosphorylation and redox activity (King, 2012).

1.2.3.2.2 Cytoplasmic dynein

Cytoplasmic dynein consists of heavy, intermediate, light intermediate and light chains which are involved in many biological processes (Figure 1.2). Cytoplasmic dynein (molecular mass of about 1.5 mega Daltons) is a complex of dimer which is composed of twelve polypeptides. Two identical heavy chains (520 kDa) regulate ATPase activity and mediate microtubule-dependent movement. The two intermediate chains (74 kDa), two light intermediate chains (53–59 kDa) and a number of light chains (McKenney *et al.,* 2014) help to attach dynein to its cargo. Cytoplasmic dynein performs enormous cellular functions (Wickstead and Gul, 2007). Cytoplasmic dynein members of mouse and human represented in Table 1.1.

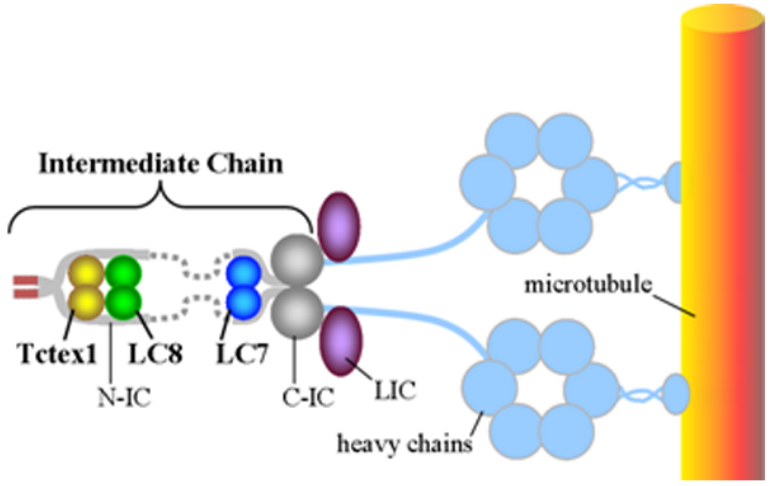

Figure 1.2: General model of cytoplasmic dynein. Structural illustration of dynein complex is adapted from *(http://www.science.oregonstate.edu/~barbare/research.html.)* Heavy chains in sky blue color shows binding to microtubule (orange). C-and N-terminals of intermediate chain are shown in gray color. Light intermediate chain is represented in purple color. Three types of light chains are illustrated in blue (LC7), green (LC8) and golden (Tctex1) colors.

Table 1.1: Cytoplasmic dynein members of mouse and human.

	Heavy Chains	Intermediate Chains	Light Intermediate Chains	Light Chains		
				Tctex1 Family	Roadblock Family	Lc8 Family
Human cytoplasmic dynein	DYNC1H1	DYNC1I1	DYNC1LI1	DYNLT1	DYNLRB1	DYNLL1
	DYNC2H1	DYNC1I2	DYNC1LI2	DYNLT3	DYNLRB2	DYNLL2
	-	-	DYNC2LI1	-	-	-
Mouse cytoplasmic dynein	DYNC1H1	DYNC1I1	DYNC1LI1	DYNLT1	DYNLRB1	DYNLL1
	DYNC2H1	DYNC1I2	DYNC1LI2	DYNLT3	DYNLRB2	DYNLL2
	-	-	DYNC2LI1	-	-	-

1.3 Heavy chain

The dynein heavy chain is a massive structure (4600 residues). The length of dynein heavy chain is greater than twice the size of myosin II and mass of kinesin. Dynein heavy chain moves along microtubule in particular directions (Ishikawa, 2012). There is a great distinction in numeral of dynein heavy chain genes in eukaryotes (Vale, 2003).

1.4 Intermediate chain

The intermediate chains DYNC1I1 (IC1) and DYNC1I2 (IC2) are involved in binding with cargo (Ha *et al.,* 2008). Interaction of dynein complex and cargo occurs in the presence of dynactin complex. Dynactin complex binds to dynein intermediate chains (DIC) to adapt dynein-cargo interactions. Dynactin complex also shows interaction with microtubule to regulate the dynein movement (Chevalier-Larsen and Holzbaur, 2006; Schroer, 2004). The intermediate chains (IC1 and IC2) are involved in direct binding with other protein cargos (beta-catenin, kinesin light chains 1 and 2, casein kinase II, huntingtin and neurofilament) (Kuta *et al.,* 2010). IC1 and IC2 possess 69% similarity and contain an approximate molecular weight of about 74 kDa (Paschal *et al.,* 1987). Intermediate chains form homo- or heterodimers (Lo *et al.,* 2006). DICs interact with dynactin through N-terminus, while its C-terminus is associated with heavy chains by means of WD40 (Ma *et al.,* 1999).

1.5 Light intermediate chain

Cytoplasmic dynein light intermediate chains (DLICs) have homology with transporter family (ABC) of ATPases. DLIC contains potential ATPase activity and acts as a novel family of dynein subunits. DLICs show complexity due to their post translational modification (Hughes *et al.*, 1995). LIC1 attaches to pericentrin (structural component of centrosome) involved in microtubule association and function (Doxsey *et al.*, 1994; Purohit *et al.*, 1999), signifying that this subunit is implicated in connecting dynein to its cargo (Purohit *et al.*, 1999; Tynan *et al.*, 2000).

1.6 Light chains

Cytoplasmic dynein contains a low molecular weight14-kDa light chain (LC) known as Tctex1. LCs function by attaching specific cargoes to the dynein complex (King *et al.*, 1996; Bowman *et al.*, 1999; Tai *et al.*, 1999). In dynein complex, three classes of LCs are well-characterized.

1.6.1 Tctex1 family

The Tctex1(t-complex testis-expressed-1) family of LCs consists of two isoforms: Dynein Light chain 1 (DYNLT1) and Dynein Light chain 3 (DYNLT3). These two isoforms help dynein to connect with its specific cargoes. DYNLT3 is involved in transportation of checkpoint proteins between kinetochore and spindle pole. DYNLT3 is also important for congression of chromosome (Lo *et al.,* 2007).

Partial structural organization of Tctex1 depicts that Tctex1 may bind directly to IC at N-terminus. Tctex1 exhibits structural similarities with LC8 despite lacking sequence similarity (Mok *et al.,* 2001). Tctex1 is involved in axonal specification, neurite development and hippocampal neurons growth (Chuang *et al*, 2005). Tctex1 acts as a component of inner arm. Tctex1 performs independent functions other than movements. Tctex1 is profusely expressed in post-mitotic neurons at embryonic stages and plays vital role in neuritogenesis (Chuang *et al*, 2005). Tctex1 expression restricts primarily to the Golgi apparatus in interphase fibroblasts (Tai *et al.,* 1999)

The human orthologous *Tcte3* gene was mapped on chromosome 6q27 (Neesen *et al*., 2002). Tcte3 encoded protein shares 87% homology. Tcte3 is mainly expressed during male germ cell development in brain, lung, and trachea tissues (DiBella *et al.,* 2001). The predominant expression of Tcte3 in somatic and male germ cells has detected by several recent studies (Huw *et al.,* 1995)

1.6.2 The Roadblock family

Dynein Light Roadblock (DYNLRB), a class of DLC has capability of modulating GTPase activity of GTP-binding proteins. Members of Roadblock family are structurally similar proteins. These proteins regulate small GTPases (Wanschers *et al.,* 2008).

1.6.3 LC8 family

DYNLL proteins were originally identified as LC. The isoforms of LC8 family are motor proteins (microtubule-based) dynein (Benashski *et al.,* 1997). DYNLL proteins are evolutionary conserved (>94% sequence similarity between *Drosophila melanogaster* and mammals) (Wilson *et al.,* 2001). Mammals articulate two strongly related isoforms: DYNLL1 (LC8a, DLC1, or PIN) and DYNLL2 (LC8b or DLC2), respectively. DYNLL2 shows 93% identity with DYNLL1 (Pfister *et al.,* 2006).

LC8 interacts with proteins having K/RSTQT or GIQVD motifs to permit their transport in a retrospective way (Navarro Lérida *et al.,* 2004).These proteins are involved in different processes including apoptosis, kidney development, enzyme regulation and viral pathogenesis (Lacy *et al.,* 2005). LC8 is a hub protein that is essential for diverse protein networks (Dunker *et al.,* 2005). The central modulatory roles of LC8 are due to its capability to endorse dimerization (Barber, 2008). LC8 functions as a cargo adapter related with both motor and cargo protein (Fan *et al.,* 2001). LC8 promotes structural stabilization and dimerization. LC8 controls binding of its partners in various protein complexes as dynein motor complex (Barber, 2008).

1.7 Apoptosis

Apoptosis is a vital constituent of a variety of processes (Cell division, chemical-induced cell death, system, hormone-dependent atrophy, embryonic development, growth and functioning of the immune system. Aberrant apoptosis causes many abnormalities in human, neurodegenerative diseases, autoimmune disorders, ischemic damage and numerous kinds of cancer (Elmore, 2007). Cell death (apoptosis) plays a crucial role in eukaryotic organisms during embryonic development and cell division.

Apoptosis prevents the organism by damaged cell, genetic mutation, aging, infection and disclosure of toxic agents (Saikumar and Venkatachalam, 2009). Apoptosis can be divided into three stages, commitment phase (extracellular or intracellular signals initiate cell death specifically), execution phase and cleanup phase (degradation in lysosomes of phagocytic cells and dead cells are removed) (Platt *et al.,* 1998). The apoptotic mechanism is conserved throughout evolution from worm to human (Yuan, 1996).

1.7.1 BCL family

The BCL-2 family proteins are involved in apoptotic processes by acting as important gatekeepers. BCL family consists of structurally similar pro-apoptotic and anti-apoptotic proteins. BCL members must have at least one BH motif (Strasser *et al.,* 2011). BCL-2 family contains 15 members in mammalian cells and numerous others in viruses (Adams and Cory, 1998). All members have four conserved domains BH1 to BH4. Most anti-apoptotic members exhibit BH1 and BH2 motifs to inhibit apoptosis. The members closely related to BCL-2 have all four BH domains (BH1-BH4). The pro-apoptotic members (Bax, Bak, and Bok) are closely related to BCL-2 and contain BH1, BH2, BH3 domains. These subfamilies differ markedly in their relatedness to Bcl-2. Bax, Bak, and Bok contain BH1, BH2, and BH3domains. In comparison, 7 other mammalian pro-apoptotic members possess only 9 to 16 AA, named as BH3 domain (Kelekar and Thompson, 1998). The BH3 domain acts as functional antagonists of anti-apoptotic proteins during programmed cell death (Conradt and Horvitz, 1998). BH3 is essential for pro-apoptotic proteins including C. elegance protein EGL-1 (Lelekar and Thompson, 1998). BCL family members (Pro- and anti-apoptotic) can heterodimerize and affect one another's function (Oltyal *et al.,* 1993).

1.7.2 Role of dynein light chains and BCL family in apoptosis

The role of motor complexes is to seize the pro-apoptotic 'BH3-only' (Bcl-2 homology 3-only) proteins, Bim (Bcl-2-interacting mediator of cell death) and Bmf (Bcl-2-modifying factor) during the regulation of apoptosis (Puthalakath *et al.,* 2004). DLC1 is a substrate of p21-activated kinase 1 (Pak1) which plays a vital role in cell survival based on phosphorylation process.

Pak1 phosphorylates Bim and prevents it from further interaction which causes inactivation of BCL-2 (anti-apoptotic protein). BCL family members (Bax, Noxa and Puma) are transcriptionally activated based on DNA damage. During apoptosis, cytoplasmic Bid moves towards mitochondria followed by cleavage (Tisujimoto and Shimizu, 2000). Bim and Bmf act in response to that apoptotic signals transmitted by apoptotic signals. Bim is involved in binding with microtubular dynein motor complex by means of LC8, while Bmf connects to myosin V actin motor complex through interaction with DLC2. These proteins are translocated to mitochondria upon apoptotic stimuli (Tsujimoto and Sujimizu, 2000). Ultraviolet (UV) radiations appear to release Bim and Bmf. These BH3-only proteins act as intracellular apoptotic sensors which induce signals to mitochondria through pro-apoptotic BCL family members having multi domains (Frisch and Screato, 2001).

1.8 Aims and objective

The major aim of current research is to identify the role of DLCs (Tcte3 and Tctex1) in programmed cell death. In order to perform these tasks, Three-dimensional structure prediction of mouse Tcte3 and Tctex1 will be carried out. The structural comparison of DLCs will enable to isolate functional relevance in motor components. Comparative molecular interaction study of LC8, Tcte3 and Tctex1 with apoptotic facilitators will be carried out to explore the functional implications of these proteins in apoptosis. The interaction assay will be elaborated through molecular dynamics simulation assays.

2. Materials and Methods

2.1 Dataset

3D structure of *rattus norvegicus* Dynein light chain 8 in complex with BCL2-LIKE 11(Bim) peptide (PDB ID: 1F95) was retrieved through Protein Data Bank (Fan *et al*., 2001). Reported binding motifs [(K/R)XTQT and G(I/V)QV(D/E)] (Puthalakath *et al*., 1999; Lo *et al*., 2001, Rodriguez-Crespo *et al*., 2001) of Dynein light chain LC8 with Bim were isolated through extensive literature survey (Rapali *et al.*,2011). 3D structure of Bim (1-9 AA) was retrieved through PDB ID: 1F95. The amino acid sequences of Tctex1 (UniProtKB - P51807, 1-113 AA) and Tcte3 (UniProtKB - P119851, 191AA) were retrieved from UniProt Knowledgebase database (Boutet *et al.,* 2016) in FASTA format. Position-Specific Iterative Basic Local Alignment Search Tool (PSI-BLAST) (Altschul *et al.,* 1990) was used against Protein Data Bank (PDB) (Sussman *et al.*, 2008) for suitable template search. The crystal structure of *Drosophila* Dynein Light chain Tctex1 (PDB ID: 1YGT) was used as template. Comparative modeling was employed to generate 3D structure of mouse Tctex1 and Tcte3 by MODELLER 9.13 (Eswar *et al.,* 2008).

2.2 3D structure modeling

In the absence of experimentally known structure, 3D structure prediction of protein from its amino acid sequence is the most important solution in computational structural biology. Under such conditions, comparative modeling is one of the most precised computational approaches to predict a consistent 3D structure from sequence information (Tramontano, 1998).

2.2.1 Comparative modeling

Due to lack of a well-defined or experimentally determined structure, protein 3D structures are predicted by homology modeling method. It is based on sequence alignment of query and target protein whose structure is experimentally resoluted (Rayan, 2009). MODELLER 9.13 (Webb and Sali, 2014) was used for homology modeling. It is a command-based tool which takes query protein sequence as input and generates an output

model for the target protein by including all non-hydrogen atoms. It employs a method known as satisfaction of spatial restraints motivated by NMR spectroscopy data processing. In MODELLER, a set of geometrical criteria is used to produce probability density functions (pdfs) for the location of each atom in the protein (Gibrat *et al*., 1996). Following five steps were involved in the model generation.

2.2.2 Sequence retrieval

Amino acid sequences of query proteins were retrieved through UniProtKB (Uniprot Consortium, 2008).

2.2.3 Template searching and selection

Retrieved sequences were subjected to PSI-BLAST (Altschul *et al.,* 1997) search against Protein Data Bank (*http://www.rcsb.org*) (Sussman *et al.,* 2008) for suitable template search. The template searching was performed by considering identity, E-value and query coverage.

2.2.4 Sequence alignment

Sequence alignment is the second step of homology modeling. In this step, query and template sequences are aligned. The significance of an alignment is usually determined by E- and p-values of the resulted sequence alignment. *Align2d* command of MODELLER 9.13 was used to align the query and template sequences. *Align2d* implements global dynamic programming with an affine gap penalty function (Eswar *et al.,* 2008) and is preferred for aligning the sequences as it tends to place gaps in a better structural context (Shen and Sali, 2006).

2.2.5 Model building

On the basis of sequence alignment between query protein and template, MODELLER 9.13 automatically calculates a model containing all non-hydrogen atoms, without any user intervention (Eswer *et al*., 2003) and a 3D model is generated. The *get-model* command was used to generate 3D models of query proteins. In total, 10 models were generated for each query protein using *get-model* command and the model with lowest

objective function among all resulted models was selected for further evaluation (Sali and Blundell, 1993).

2.2.6 Model evaluation and refinement

For model evaluation, model quality and potential errors in 3D models were assessed through different web servers ProSa-web (Wiederstein and Sippl, 2007), ERRAT (Colovos, 1993), VERIFY 3D (Eisenberg *et al*., 1997), RAMPAGE (Lovell *et al.,* 2003) and MolProbity (Chen *et al.,* 2010). The recognized tool ProSA often used in refinement, validation of experimental protein structures and *in-silico* protein modeling by means of Z-score representation. The model quality evaluates through Z-score by comparing with known protein structures (Z-score). The evaluated Z-score must be within the range of value for similar size protein chains. ERRAT uses a novel method for differentiating between correctly and incorrectly determined regions of protein structures based on characteristic atomic interaction. ERRAT quadratic error function is used to characterize the set of pairwise interactions from nine-residue sliding windows in a database of 96 reliable protein structures (Colovos and Yeates, 1993). Verify 3D assigns a structural class on the basis of location and environment to determine the compatibility of 3D model with its own 1D primary sequence. RAMPAGE generated a Ramachandran plot and provides information about favored, allowed and outlier regions. The structure validation tool MolProbity evaluates proteins on both local and global level. MolProbity relies on power and sensitivity provided by optimized hydrogen placement and all-atom contact analysis, covalent-geometry and torsion-angle criteria (Chen *et al.,* 2010). Model refinement and geometry optimization was done by WinCoot (Emsley *et al*., 2010) and UCSF Chimera 1.8.WinCoot displays maps and models and allows model manipulations such as idealization, real space refinement, manual rotation/translation, rigid-body fitting, ligand search, solvation, mutations, rotamers, Ramachandran plots, skeletonization, and non-crystallographic symmetry (Lohkamp *et al*., 2005). UCSF Chimera 1.8 is an extremely extensible program for interactive visualization and analysis of molecular structures, including density maps, supra-molecular assemblies, sequence alignments, docking results, trajectories, energy minimization and conformational ensembles (Pettersen *et al*., 2004).

2.3 Multiple and pairwise sequence alignment

Multiple and pairwise sequence alignment was carried out for Tctex1 and Tcte3 with 1YGT and LC8. Multiple sequence alignment was done for Tctex1 and Tcte3 to inspect the sequence similarity of the proteins with selected template IYGT using CLC Main Workbench. Pairwise alignment for Tctex1 with LC8 and Tcte3 with LC8 was carried out using EMBOSS needle (Li *et al.,* 2015) to explore the similarity of the proteins at sequence level.

2.3.1 CLC Main Workbench.

CLC Main Workbench is used by tens of thousands of researchers all over the world for DNA, RNA, and protein sequence data analysis (Workbench, 2010).

2.3.2 Emboss Needle

Emboss needle requires two input FASTA sequences and marks their optimal global sequence alignment to output file. It works on the Needleman-Wunsch alignment algorithm for obtaining optimum alignment (including gaps) of two sequences along their entire length. The algorithm uses a dynamic programming method by exploring all possible alignments to ensure the optimal alignment.

2.4 Molecular docking

To obtain best native conformation and predict a reliable interaction, computational approach (Protein-Protein docking) was employed to examine the binding region of respective proteins (Tctex1 and Tcte3). The molecular docking was performed by using AutoDock tools 4 (Morris *et al*., 2009), AutoDock Vina (Trott and Olson, 2010), ClusPro (Kozakov *et al.*, 2013) and HADDOCK (de Vries and Bonvin, 2011) to identify binding grooves of Tctex1 and Tcte3 against Bim peptide (apoptotic facilitator) as well as for homodimerization.

2.4.1 AutoDock4 and AutoDock Vina

AutoDock is a suite of automated docking tools. It is designed to predict how small molecules, such as substrates or drug candidates bind to a receptor of known 3D structures. Current AutoDock distribution comprises two generations of software (AutoDock4 and AutoDock Vina). AutoDock Vina significantly improves the average accuracy of the binding mode predictions compared to AutoDock4. In AutoDock4 and AutoDock Vina analysis, ligand and receptor molecules were prepared by assigning kollman charges and adding polar hydrogen atoms. The docking experiments were performed with a rigid receptor and flexible ligands by allowing all torsions to rotate. In AutoDock4, for each ligand 100 independent docking runs were carried out with a grid map and spacing in Angstroms (Å). The empirical free energy function and Lamarckian genetic algorithm (LGA) was applied with the following parameters: a population of 150, maximum number of 27,000 generations, a mutation rate of 0.02, crossover rate of 0.80 and number of energy evaluations was 2.5×10^6. The remaining docking parameters were set to default. Subsequently, results were clustered according to RMSD criterion and the ideal docked conformations of ligands were selected on the basis of binding free energy values to evaluate Tctex1 and Tcte3 binding with Bim. The best docked complex for each ligand was selected and interactions were monitored using DIMPLOT (Wallace *et al*., 1995) which generated a plot of interactions.

2.4.2 HADDOCK

HADDOCK is a popular docking program that takes a data-driven approach for docking, with support for a wide range of experimental data. HADDOCK is the combination of two computational approaches, interface prediction and docking to obtain atomic-level structures of protein-protein complexes. The HADDOCK server has access to the resources of a dedicated cluster and of the e-NMR GRID infrastructure. Therefore, a typical docking run takes only a few minutes to prepare and a few hours to complete (De Vries *et al.,* 2010). Interface prediction comprises a set of optimal restraints for data-driven docking using HADDOCK. The six interface prediction web servers are combined in a consensus method called CPORT (Consensus Prediction Of interface Residues in

Transient complexes). CPORT predictions were used to dock the full protein-protein benchmark, excluding only antibody-antigens and multimer complexes, using HADDOCK. CPORT predictions were shown to be more reliable and resulted in at least an acceptable docking solution in the top 400 for the majority of the complexes (de Vries and Bonvin, 2011). In first step, tertiary structures of Tctex1,Tcte3 and Bim were submitted to CPORT server for prediction of interface residues (active and passive).These residues were utilized as input in HADDOCK. Similarly, in case of dimerization, two monomers of each protein were submitted to HADDOCK after CPORT. The top ranked clusters were selected for further experimentation.

2.4.3 ClusPro

ClusPro is a docking tool which rapidly filters the output from the Fourier correlation algorithm using a combination of desolvation and electrostatic energies (calculated using a Coulomb potential). This approach results in several near-native structures passing through the filter, while eliminating many of the false positives. To monitor the interaction, docking analysis was also performed through ClusPro (Kozakov *et al.*, 2013). ClusPro uses three main steps, a rigid body docking program (PIPER) based on novel Fast Fourier Transform (FFT) technique with pairwise potential. The 1000 suitable energy conformations are clustered and 30 largest clusters are retained for refinement by detecting native and non-native clusters. The stability of clusters is analyzed by Monte Carlo simulations and refinement is performed by SDU (Semi-Definite programming based Underestimation). In ClusPro, input PDB files were of Tcte3, Tctex1 and Bim, which resulted in four predicted models (Balanced, Electrostatic-favored, Hydrophobic-favored and VdW+Elec). Models were ranked by cluster size and lowest binding energy values.

2.5 Molecular dynamics simulation assay

Molecular Dynamics (MD) simulation of suitable docked complexes was performed by GROMACS 5.7.4 version (Schumann-Gillett *et al.,* 2017). GROMACS is a high end, high performance research tool designed for the study of molecular dynamics. Best

docked complexes Tctex1-Bim and Tcte3-Bim were subjected to GROMACS for molecular dynamics simulation analysis. A detailed analysis was performed to evaluate the conformational changes, folding, stability, and dynamic behavior of interacting proteins. All MD simulations were performed on highly efficient OpenSuse Linux system using Amber03 force field by GROMACS. MD simulation assay consists of three stages: First, preparation of simulation system. Second, the simulation run and third one the results have to be analyzed.

2.5.1 PDB complex file preparation

Before MD simulations, the complex was needed to be optimized. AutoDock4 was used to check any missing atom and to repair the missing atoms in the complex.

2.5.2 Topology file generation

Since the structure of protein complex obtained through molecular docking only contains coordinates, there is a need to build the topology, which illustrates the system in terms of atom types, charges and bonds etc. This topology is specific to a certain force field. We used AMBER03 force field (Duan *et al.,* 2003), which fits the dihedral potentials to new structure to construct the topology. The *pdb2gmx* command was used to build topology file for molecules consisting of distinct building blocks (amino acids). The topology file is very important as it contains all the force field parameters and the respective hydrogen atoms according to the chosen force field. AMBER03 force field and Tip4p water model was selected.

2.5.3 Periodic boundary conditions and salvation

Before adding the solvent, a general layout (space/box) of the simulation setup had to be chosen. Most frequently, simulations are performed under periodic boundary conditions (PBC). A single unit cell is defined, which can be stacked in a space filing manner. In this way, an infinite periodic system can be simulated by avoiding edge effects due to walls of simulation volume. There are only a few general shapes available to set up PBC. We selected the octahedron unit cell. To disallow direct interactions among periodic images,

a minimal distance of 1.0 Å was set between protein and wall of cell (the two neighbors should not be closer than 2.0 nm). PBCs were set with *editconf* command. After the unit cell setup, solvent was added. There are several solvent models, each of which is more or less intimately linked to a force field. Amber03 force field is generally used with Tip4p water model.

2.5.4 Addition of ions: counter charge and concentration

After solvation, system contains charged proteins. Total charge on the system was calculated and system was neutralized by adding counter ions to solution.

2.5.5 Energy minimization and evaluation

After neutralization, next step was to minimize the energy of system to 500 steps through steepest descent algorithm, by a tolerance of 1000 kJ/mol$Å^2$. PBCs were applied in all directions. Normally, the system needs to be minimized in order to remove any local strains. These strains are result of small errors in the original structure such as Vander Walls contacts. Even small differences between GROMACS force field to improve PDB structures lead to unrealistically high forces among atoms. By energy minimization (EM), clashes can be removed.

To evaluate the success of EM, two important factors are used. The first one is potential energy (indicated at the end of the EM process). The potential energy should be negative for an apo protein or protein complex in water. It depends on the system size and the number of water molecules. The second important attribute is the maximum force (Fmax), the target for which it is defined by minim.mdp- "emtol = 1000.0 (representing a target Fmax of no greater than 1000 kJ $mol^{-1}nm^{-1}$).

2.5.6 Equilibration

Following the minimization step, system was subjected to equilibration for 1000 ps under constant temperature (300 K). The pressure was set to 1 ATM in NVT (isothermal-isochoric, constant number of particles, volume, and temperature) and NPT (isothermal-

isobaric) ensemble, with a time step of 2 fs for geometric integration with leap frog algorithm.

2.5.7 MD simulation run

Finally, the system was ready to run simulations. MD runs for 20 ns time scale under constant temperature and pressure conditions were performed. Particle Mesh Ewald (PME) algorithm (Abraham and Gready, 2011) was used to calculate long range electrostatic interactions.

2.5.8 Analysis of simulations

Trajectories were analyzed by using tools embedded in GROMACS package. Snapshots were collected throughout MD simulations of each system and PDBs were generated for 1, 5, 10, 11, 15, 18 ns intervals to investigate the time-dependent behavior and stability of each system. GROMACS and UCSF Chimera were used to analyze the stability and behavior of each system.

3. RESULTS

3.1 Modeling of dynein light chains: Tctex1 and Tcte3

Due to absence of experimentally known structures, a comparative modeling technique was utilized to predict 3-dimensional structures of mouse Tcte3 and Tctex1. The retrieved amino acid sequences of Tctex1 and Tcte3 were subjected to PSI-BLAST for suitable template search. The crystal structure of *Drosophila* Dynein Light chainTctex1 (PDB ID: 1YGT) was selected as an appropriate template on the basis of sequence identity and query coverage with target sequences (Table 3.1).

Table 3.1: Template selection for Tctex1 and Tcte3. Template sorted by overall query coverage, e-value and identity against target proteins.

Targets	Template (PDB ID)	Query Coverage	E-value	Identity
Tctex1	1YGT	100%	4e-55	67%
Tcte3	1YGT	67%	0.053	20%

The sequence and structural comparison of target proteins with template was observed by multiple sequence alignment and structural superimposition (Figure 3.1). The multiple sequence alignment between Tctex1, Tcte3 and 1YGT revealed 80-100% conservation. Tctex1 and Tcte3 exhibited high structural conservation with *Drosophila* Dynein Light chain Tctex1. The superimposition of template and target proteins was based on their C-alpha or backbone atoms. The superimposed structures (1YGT-Tctex1 and 1YGT-Tcte3) exhibited RMSD values of 0.316Å and 1.167Å, respectively. Energy minimization was applied on the predicted models to improve their stereochemistry and to remove the energy constraints. The stereochemistry of Tctex1 and Tcte3 significantly was improved. The minimization was performed using ff99SB forcefield with AMBER parameters. The predicted 3D models for Tctex1 and Tcte3 were validated through different evaluation tools.

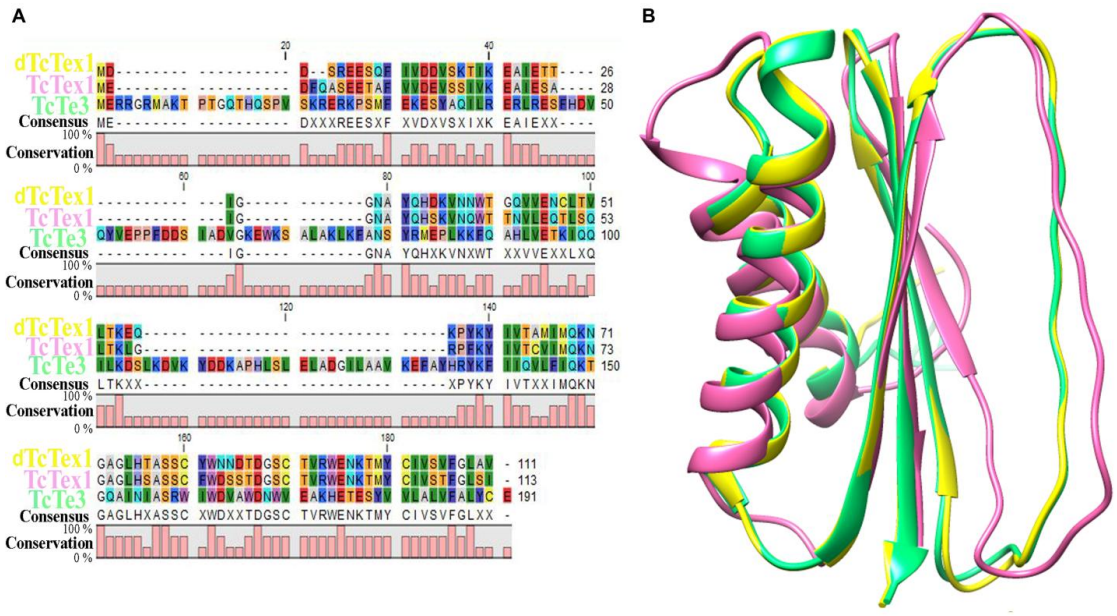

Figure 3.1: Tctex1 and Tcte3 structural overlap with template. (A) Amino acid sequence conservation of Tcte3, Tctex1 and *Drosophila* dynein light chain Tctex1 (PDB ID: 1YGT). (B) Superimposition of target (Tcte3: spring green), (Tctex1: hot pink) and template (1YGT: yellow) structures.

3.1.1 Model evaluation

The 3D structures were validated through geometrical analysis. The analysis included rotamer evaluations, ramachandran plots and Cβ deviations. The overall geometry of models including residual distribution is represented in Table 3.2.

Table 3.2: Evaluation of predicted 3D structures of Tctex1 and Tcte3.

Sr. #	Protein Geometry	Tctex1	Tcte3
1	Poor Rotamers	0.00%	0.00%
2	Favored Rotamers	94.95%	83.33%
3	Ramachandran Outliers	0.00%	0.98%
4	Ramachandran Favored	99.10%	84.35%
5	Cβ deviations >0.25Å	0.94%	8.82%
6	Bad Bonds	0.00%	0.23%
7	Bad Angles	0.83%	2.41%

The overall model quality was assessed by Z-score. The calculated Z-score value measures the energy divergence of structure against energy distribution resulting from random conformations. The Z-scores for predicted Tctex1 and Tcte3 models determined the separation between native folds and misfold assembly on the basis of standard deviation unit assembly. The calculated Z-scores for Tctex1 (-5.28) and Tcte3 (-3.47) validated the abilities of knowledge-based potentials. The Z-score was calculated to identify the native folds. The 3D predicted models for Tctex1 and Tcte3 were subjected to ERRAT protein structure verification server. A 9-residue sliding window used quadratic error function to distinguish the pairwise interactions. ERRAT provided overall quality factor for both models was greater than 70%. The ERRAT values differentiated the correct and incorrect regions of protein structures on the basis of atomic interactions.

The RAMPAGE gave results in the form of Ramachandran plots. Ramachandran plot exhibits the residual and phi (Φ)and psi (Ψ) angle distribution against non-Proline and non-Glycine residues. The phi and psi angles were used to assess the distinction of favored and unfavored regions. In Ramachandran analysis, 99% and 85% residues of Tctex1 and Tcte3 were lying in most favored regions, respectively.

3.2 Comparative sequence and structural characterization of LC8, Tctex1 and Tcte3

Dynein light chains (LC8, Tctex1 and Tcte3) were compared at sequence and structure level to elucidate the similarities among LC8, Tctex1 and Tcte3 which might be useful to deduce functional relevance. The pairwise sequence alignment was used to compare primary sequences of dynein light chains (Tctex1, Tcte3 and LC8). The superimposition of 3D structures of focused dynein light chain complexes (LC8-Tctex1 and LC8-Tcte3) was performed to infer suitable structural and functional conservation of Tctex1, Tcte3 with LC8. This analysis suggested that LC8-Tctex1 was more conserved than LC8-Tcte3 at sequence level. However, LC8, Tctex1 and Tcte3 light chains were more conserved at structural level than sequence. The LC8-Tctex1 pairwise sequence alignment exhibited an alignment score of 15.5%, while superimposition of LC8 and Tctex1 yielded an RMSD value of 1.412 Å. In case of LC8-Tcte3 superimposition, the RMSD value (0.953Å) was considered more reliable for Tcte3 structural similarity with LC8 than

Tctex1. The pairwise sequence alignment of LC8 and Tcte3 revealed an alignment score of 13.0%. Tctex1 and Tcte3 exhibited elongated β-sheets as compared to LC8. Dynein light chain LC8 consists of two α-helices and four β-sheets named as β1, β2, β3 and β4 (Figure 3.2). The Tctex1 and Tcte3 followed the same topology as LC8 with differences in the number of β-sheets. Hence, structural comparison is a clear approach to deduce the functional propensities of light chains.

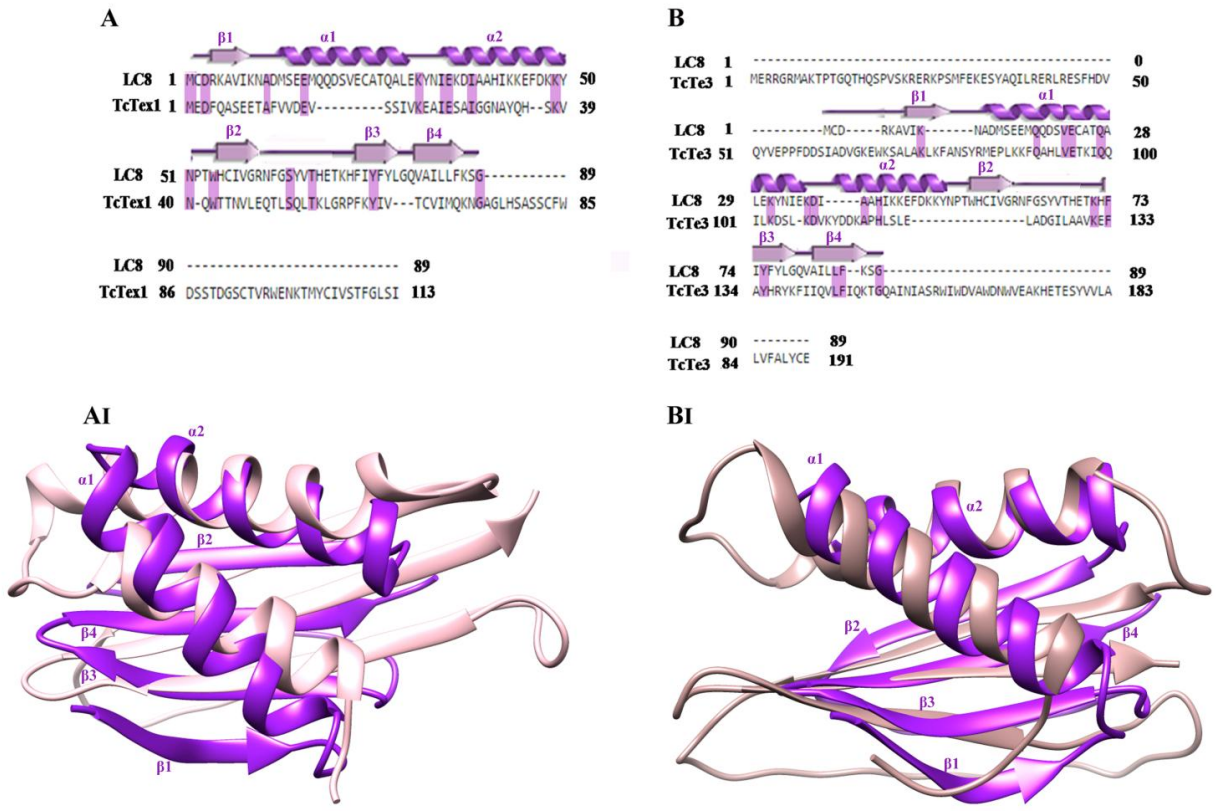

Figure 3.2: Pairwise sequence alignment and superimposition of three-dimensional structures (3D) of LC8, Tctex1 and Tcte3. (A) Pairwise sequence alignment of LC8 and Tctex1. Conserved residues are shown in light purple shade. Secondary structures (Coils, Strands and helices) of LC8 are drawn and labeled in purple color. **(B)** Superimposition of LC8 with Tctex1 is represented in purple and pink color. Secondary structures are mentioned in purple color. **(AI)** Pairwise sequence alignment of LC8 and Tcte3. Conserved residues are shown in light purple shade. Secondary structures (Coils,

Strands and helices) of LC8 are drawn and labeled in purple color. **(BI)** The superimposition of LC8 with Tcte3 is represented in purple and rosy brown color. Secondary structures are labeled in purple.

3.3 Structural insights of LC8, Tctex1 and Tcte3 dimerization

The critical regulatory role of LC8 in a variety of systems is due to its capability to endorse dimerization of chaotic proteins (Barbar, 2008). The crystallographic and NMR studies exposed that Bim, nNOS and Swallow bind to LC8 dimer in the vicinity of binding grooves. The past studies revealed binding at dimer interface (Fan *et al., 2001*; Benison *et al.,* 2007). LC8 acts as a dimerization engine in dynein (Makokha *et al.,* 2002). In the reported LC8-Bim RAT dynein motor complex (PDB ID: 1F95), LC8 dimer conformation contains two pairs of α-helices covering in opposite faces, and each pair of helices packs against a β-sheet with 5 antiparallel β-strands. Each 5-stranded β-sheet exhibits 4 strands from one monomer and a 5th strand from the other monomer. A 13-residue peptide from nNOS is bound to the dimer in the deep hydrophobic groove as a 6th antiparallel β-strand (Liang *et al.,* 1999). LC8 exists as a homodimer both in the absence and presence of its target proteins. LC8 dimer displays a rectangular symmetry due to extensive hydrogen bonds and hydrophobic interactions of both monomers.

To elucidate the dimer orientation of mouse Tcte3 and Tctex1, their models were subjected to docking analysis. The resulted dimers adopted similar orientation as reported structures of LC8 (PDB ID : 1F95; Fan *et al.,* 2001) and human LC8-Bim complex (PDB ID: 1CMI; Liang *et al.,* 1999). In rat LC8 dimer (1F95), β2-strand of one monomer was linked with β2-strand of other monomer through hydrogen bonding. Gly63 and Cys56 residues of one monomer were involved in hydrogen bonding with Val58 and Tyr65 of second monomer (Figure 3.3). The conformational topology of crystallographic structure (LC8-Bim) complex exhibited two grooves at opposite sides of dimer interface.

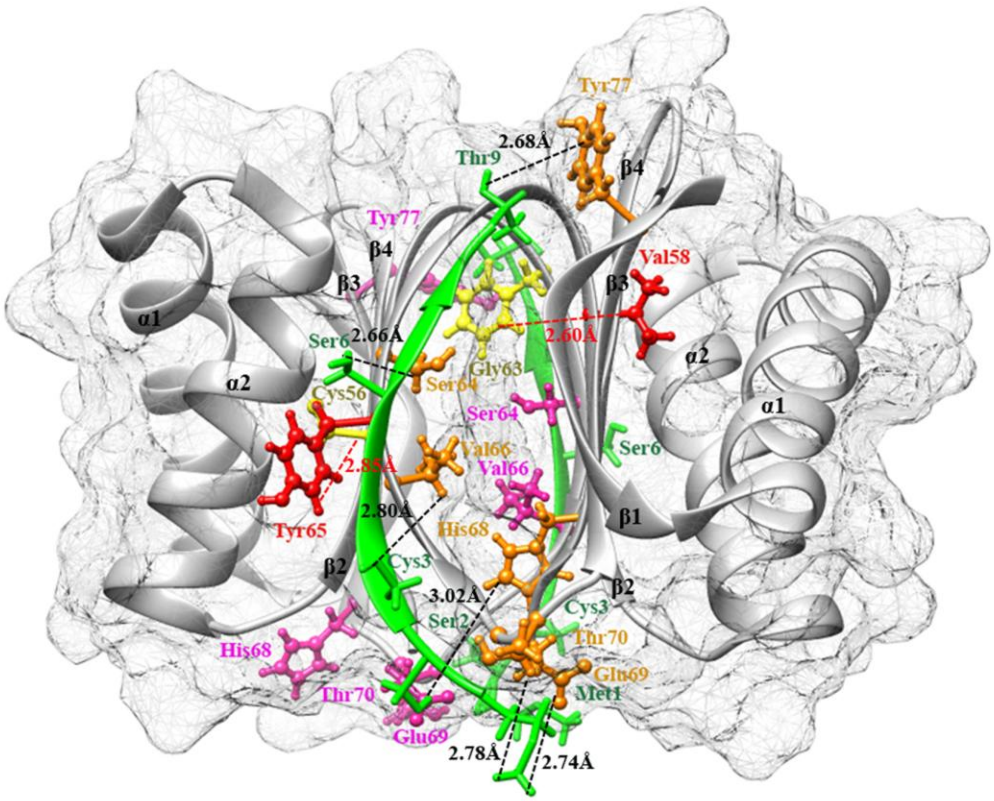

Figure 3.3: Dimer of LC8. The docked monomers of LC8 are represented in gray color mesh surface. Bim peptides are shown in green color. The residues of one monomer are illustrated in yellow and hot pink colors, yellow residues are involved in binding with other monomer residues (red) for dimerization and hot pink residues are involved in binding with Bim. Residues of other monomer are indicated in red and orange colors. The residues of monomer in orange color are represented the interactions with Bim. Hydrogen bonds are drawn and labeled in black for LC8-Bim interaction and red color indicated LC8-LC8 hydrogen bonding. Secondary structure elements are labeled in black.

In Tctex1 dimer, the binding groove at dimer interface was similar to LC8 and Tcte3 (Figure 3.4). The investigation of Tctex1 dimer interface exhibited uniform pattern of interaction between both monomers. Consequently, from one monomer Ser107, Ser88 and Asp86 residues were implicated in hydrogen bonding with His78, Asn73 and Gln71 residues of the other monomer. Hence, residues of one monomer were located at β-strands and loop region, which manifested the interactions with residues at β-strand and

loop region of other monomer. In case of Tctex1 dimer interaction with Bim some conserved residues (Ser81, Ser82, Cys83, Phe84 and Trp85) were observed.

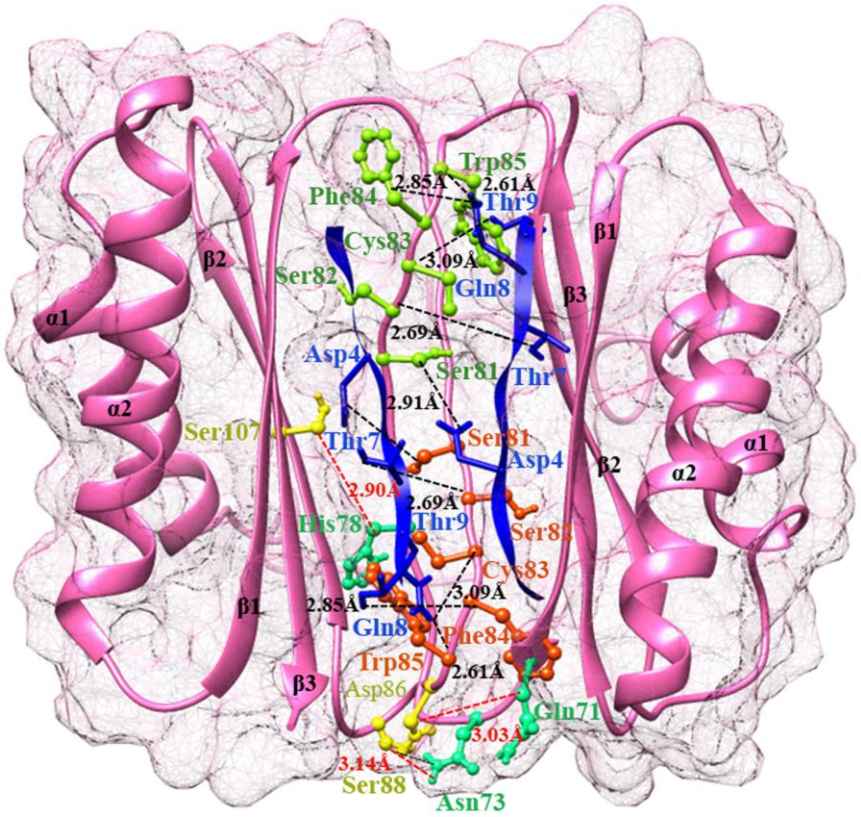

Figure 3.4: Dimerization of Tctex1. The docked monomers of Tctex1 are represented in mesh surface representation (hot pink color). Bim peptides are shown in blue color. The residues of one monomer are illustrated in yellow and orange colors, which are involved in binding with other monomer (yellow) and Bim peptide (orange). Residues of other monomer are indicated in spring green and dark green colors. The spring green residues of monomer are represented interactions with other monomer residues (yellow) and dark green color with Bim residues (blue). Hydrogen bonds are drawn and labeled in black for Tctex1-Bim and red color indicates Tctex1 monomers interactions. Secondary structure elements are labeled in black color.

The Tcte3 dimer form exhibited 4 β-sheets (Figure 3.5). β2-strand was converted into loop region, which was engaged in dimerization. The residues of one monomer (Asp124,

Phe140, Ile142 and Gln152) were involved in hydrogen bonding with second monomer residues (Ala157, Arg159, Gln143 and Asp113). In Tcte3 dimer few conserved residues (Asn155, Ile156, Ser158, Trp160 and Asp163) were involved in binding with Bim to form a ternary complex.

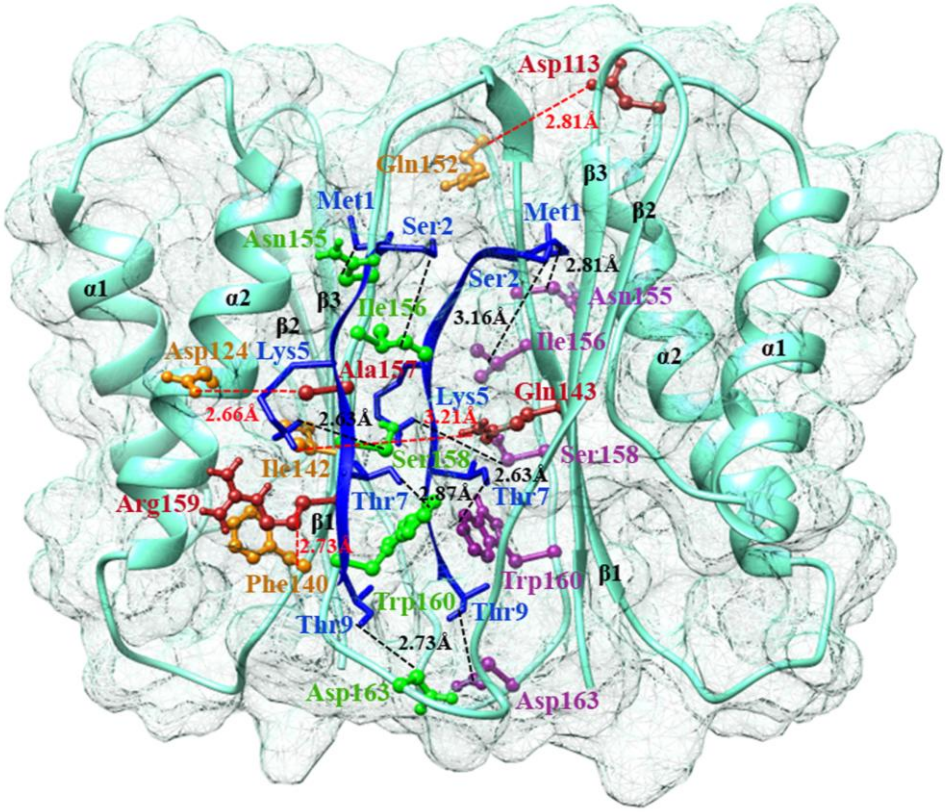

Figure 3.5: Dimerization of Tcte3. The docked monomers of Tcte3 are represented in mesh surface representation (aquamarine color). Bim peptides are shown in blue color. The residues of one monomer are illustrated in brown and green colors, which are involved in binding with other monomer (brown) and Bim peptide (green). Residues of other monomer are indicated in orange and purple colors. The orange residues of monomer represent the interactions with other monomer residues (brown) and purple residues with Bim (blue). Hydrogen bonds are drawn and labeled in black for Tcte3-Bim and red color indicates Tcte3 monomers interactions. Secondary structure elements are labeled in black color.

3.4 Binding mode of Tctex1 and Tcte3 against apoptotic facilitator

In current study, our goal is to investigate the binding grooves of Tctex1 and Tcte3. The docking analysis of Tctex1 and Tcte3 dimers against pro-apoptotic facilitator (Bim peptide) was performed. The analysis was investigated the binding grooves of Tctex1, Tcte3 for Bim peptide and homodimerization (Figures 3.6 and 3.7). We mapped binding of Bim with dimer form of Tctex1 and Tcte3 to monitor their binding grooves. We encapsulated the major interactions between Tctex1, Tcte3 and Bim peptide. The target Bim peptide accomplished the formation of antiparallel β-strand to the pre-existing β-sheets of Tctex1 and Tcte3, resulting in a tetrameric complex (Figure 3.4 and 3.5). These results were remarkably firm with the previously known ternary complex of LC8-Bim dimer. The analysis revealed that dimerization interface and Bim peptide binding groove attain similar topology in dynein light chains.

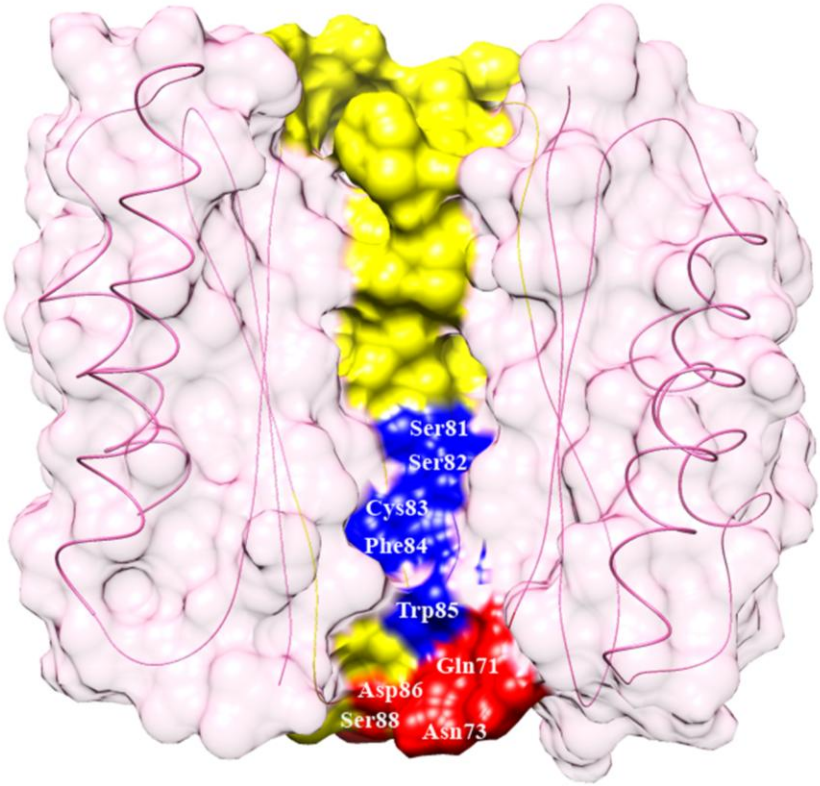

Figure 3.6: Binding groove of Tctex1. Surface representation of Tctex1 in hot pink color. Ribbons are shown in licorice ribbon style. Yellow surface illustrates the binding

groove of Tctex1. The conserved residues of Tctex1 groove for Bim target peptide are shown in blue color. Red color representation indicates the groove region which involved in Tctex1 homodimerization. Residues are labeled in white color.

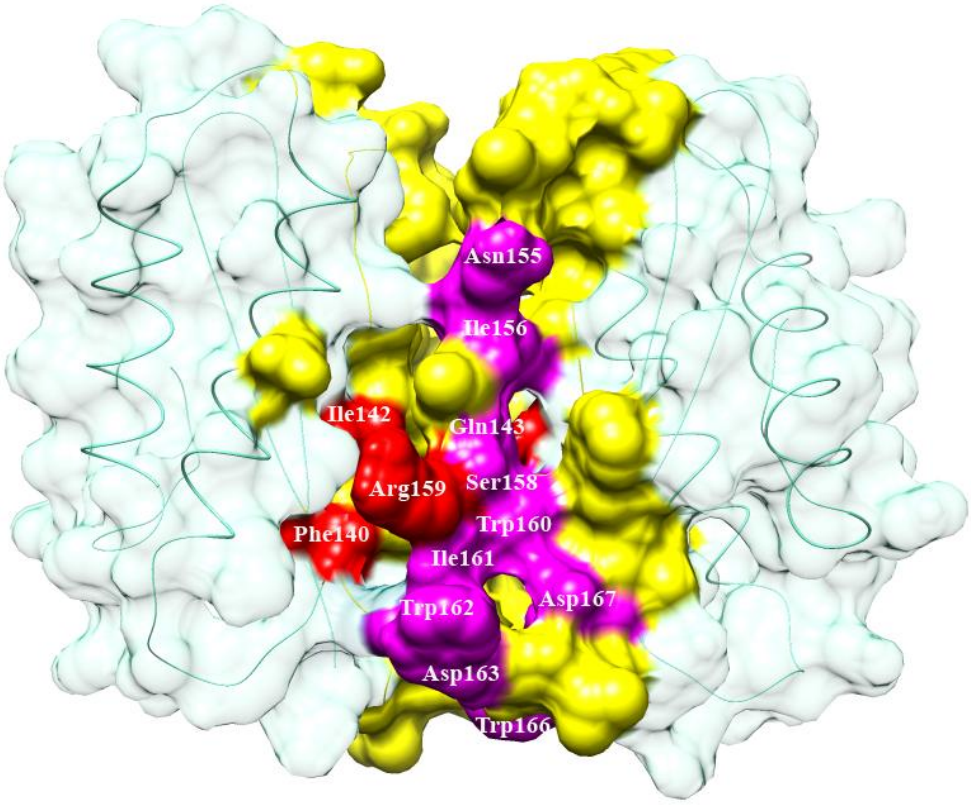

Figure 3.7: Binding groove of Tcte3. Tcte3 is shown in surface (aquamarine color) and in licorice ribbons form. Yellow dark surface indicates the binding region. Residues are shown in violet red color which represents interaction with Bim and residues in red color are represented the binding groove for Tcte3 homodimerization. Residues are labeled in white color.

3.5 Comparative binding mode analysis for Tcte3 and Tctex1

In order to characterize the binding of Bim with Tcte3 and Tctex1, initially, we evaluated known apoptotic complex of LC8 and Bim (Rapali *et al*., 2011) via docking analysis. These observations led us in establishing training data set and docking protocol for comparative docking analysis of Tctex1 and Tcte3 with apoptotic factor Bim (Figure

3.8). The findings were ranked on the basis of lowest energy values (Tables 3.3 and 3.4) for detailed analysis.

Table 3.3: Comparative binding analysis of Tctex1 with Bim. Comparative binding energies (B.E) and residues of Tctex1 and Bim obtained by utilization of AutoDock (AD), AutoDock Vina (AD Vina), ClusPro (CP) and HADDOCK (HD). Conserved residues are involved in binding mentioned in bold.

Complexes	**Tctex1 Residues**	**Bim Residues**	**B.E (Kcal/mol)**	**Hydrogen Bonds (Å)**
Tctex1-Bim-AD	Phe12, Val14, Asp15, Ser18, Lys22, **Ser81, Ser82, Cys83, Phe84, Trp85, Ser92, Cys93**, Val95, **Arg96**	Met1, Ser2, Cys3, Asp4, Lys5, Thr7, Gln8, Thr9	-3.63	Lys22**:** Ser2 Asp15**:** Cys3 Ser92**:** Asp15 Trp-85**:** Gln8 Cys83: Thr9
Tctex1-Bim-AD Vina	Phe12, Val14, Asp15, Ser18, Lys22, **Ser82, Cys83, Phe84, Trp85, Ser87, Ser92, Cys93**, Val95, **Arg96**	Met1, Ser2, Cys3, Asp4, Lys5, Thr7, Thr9	-10.7	Ser92: Asp4 Asp15: Cys3 Ser87: Ser6
Tctex1-Bim-CP	Leu77, Ser79, Ala80, **Ser81, Ser82, Cys83, Phe84, Trp85, Ser87, Ser92**, Thr94, Phe109	Ser2, Cys3, Asp4, Lys5, Ser6, Thr7, Gln8, Thr9	-648.8	Ser79: Ser2 Ser81: Asp4 Ser82: Thr7 Phe84: Gln8
Tctex1-Bim-HD	Val17, Tyr63, Met70, Lys72, Gly74, Ala75, Gly76, Leu77, Ser79, **Ser81, Ser82**, **Trp85**, **Ser87**, Thr89, Asp90, Gly91, **Ser92**, **Cys93**, Thr94, **Arg96**, Tyr103, Ile105, Thr108, Gly110	Met1, Ser2, Cys3, Asp4, Lys5, Ser6, Thr7, Gln8, Thr9	-68.5	Ala75**:** Met1 Leu77**:** Met1 Ser79**:** Cys3 Thr94**:** Ser6 Ser81**:** Lys5 Ser92**:** Thr7 Gly110**:** Thr9 Thr89**:** Thr9

Table 3.4: Comparative binding analysis of Tcte3 with Bim. Comparative binding energies (B.E) and residues of Tcte3 and Bim obtained by utilization of AutoDock (AD), AutoDock Vina (AD Vina), ClusPro(CP) and HADDOCK(HD). Conserved residues are involved in binding mentioned in bold.

Complexes	**Tcte3 Residues**	**Bim Residues**	**B.E (Kcal/mol)**	**Hydrogen bonds (Å)**
Tcte3-Bim-AD	Leu145, Phe146, Ile154, **Asn155, Ile156**, Ser158, **Trp160**, Val164, **Asp167**, Asn168, **Trp169**, Tyr189	Met1, Ser2, Cys3, Asp4, Lys5, Ser6, Thr7, Gln8, Thr9	-5.9	Ile156: Ser2 Trp169: Ser6 Ile154: Met1 Asn155: Ser2 Asp167: Thr7
Tcte3-Bim-AD Vina	**Lys87**, Lys88, **Trp160**, **Ile161**, **Trp162**, **Asp163**, Ala165, **Trp166**, **Asp167**, **Trp169**, Glu171, Lys173, Leu188	Met1, Ser2, Cys3, Lys5, Ser6, Thr7, Gln8, Thr9	-9.9	Trp169: Lys5 Asp167: Cys3
Tcte3-Bim-CP	**Lys87**, Leu145, Phe146, Ile147, Ile154, **Asn155**, **Ile156**, Ser158, **Trp160, Ile161, Trp162, Asp163, Trp166, Asp167**, **Trp169**, Leu182, Phe186	Met1, Ser2, Cys3, Asp4, Lys5, Ser6, Thr7, Gln8, Thr9	-701.5	Asn155: Met1 Ile156: Cys3 Ser158: Lys5 Asp167: Thr9 Asp163: Thr9
Tcte3-Bim-HD	**Lys87**, Ile141, Ile147, Ala153, **Asn155, Ile156**, **Trp160, Ile161**, **Trp162**, **Asp163, Trp166**, **Asp167**, Asn168, **Trp169**, Lys173, Leu184, Leu188	Met1, Ser2, Cys3, Asp4, Lys5, Ser6, Thr7, Gln8, Thr9	-124.4	Trp166: Met1 Asp163: Ser2 Asp167: Lys5 Trp160: Cys3 Ile156: Ser6 Asn155: Thr7 Trp169: Ser6 Lys87: Gln8 Lys173: Thr9

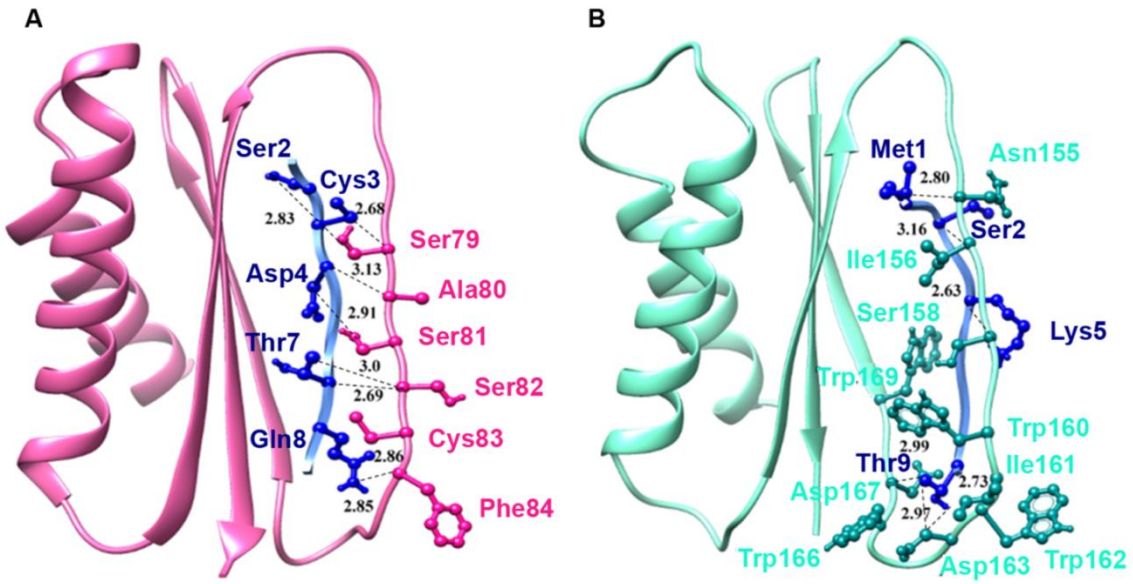

Figure 3.8: Molecular interaction analysis of Tctex1 and Tcte3 with Bim. (A) Interaction analysis of Tctex1 (pink ribbons) and Tcte3 (turquoise ribbons) with Bim (cornflower blue). (B) The binding pocket residues of Tctex1 (deep pink) and Tcte3 (dark cyan) involved in Bim (cornflower blue ribbons, blue residues) interaction are indicated in ball and stick representation. Conserved binding residues of Tcte3 and Tctex1 are represented in dark cyan and hot pink, while Bim residues are labeled in blue color.

The detailed binding residues of individual apoptotic factor (Bim) with Tctex1 and Tcte3 were depicted in Tables 3.4 and 3.5. LC8 conserved residues (Thr70, Glu69, Val66, His68, Ser64, Phe62 and Tyr77) lie at β2-L4-β3 region are involved in interactions with Bim (Fan *et al.*, 2001). In case of Tcte3 and Tctex1, binding of Bim peptide was detected at the similar regions in Tcte3 and Tctex1. Tctex1 specific Ser81, Ser-82, Cys-83, Phe-84, Trp-85, Ser-92, Arg-96 and Ser87 residues were involved in binding with Bim (Figure 3.8A), while binding region of Tcte3 was comprised of Asn155, Ile156, Trp160, Asp167, Trp169, Lys87, Ile161, Trp162, Asp163 and Trp166 residues (Figure 3.8B).

3.6 Molecular dynamics simulation analysis

Elucidation of conformational changes, stability and dynamic behavior of respective protein complexes (Tcte3-Bim and Tctex1-Bim) were observed by MD simulation assays. Consequent trajectories were meticulously analyzed to estimate constancy, junctions, vigorous, functional and structural characteristics while running simulations.

3.6.1 Root mean square deviation analysis of Tctex1 and Tcte3

Time succession of root mean square deviation (RMSD), root mean square fluctuation (RMSF) were evaluated to predict the stability and fluctuations of C-alpha atoms in bound and Apo forms. The overall stability of each complex was deliberated by calculating the RMSD profile (Figures 3.9 and 3.10). RMSD for each complex was intended by means of apo-form as a reference. The average RMSD values of respective protein complexes Tcte3-Bim with apo-Tcte3 (1.114 Å) (Figure 3.9A) and Tctex1-Bim with apo-Tctex1 (1.20 Å) (Figure 3.10A) represented a stable environment of systems.

3.6.2 Root mean square fluctuation analysis of Tctex1

RMSF values calculate the degree of residual fluctuations, which were reprsented by peak altitude in graphs (Figures 3.9B and 3.10B). In Tctex1-Bim complex, major fluctuations were present in residues namely Gln35 (0.1728 Å), His36 (0.1848 Å), Lys72 - His78 (0.1824-0.3403 Å) and Thr101 (0.1626 Å) (Figure 3.9B). These fluctuations were located in the loop regions except His-36 that fluctuated in α1 (Figure 3.9B). However, interacting residues involved in binding with Bim peptide (Lys62, Ile64, Thr66, Val68, Ile69, Met70, Gln71, Leu77, Ser79, Ala80, Ser81, Ser82, Cys83, Phe84, Ile105, Ser107, Phe109 and Leu111) were stable except Leu-77. The Leu77 was fluctuated in loop4 region and it was considered as less stable. Tctex1 conserved residues (Ser81, Ser82, Cys83, Phe84, Trp85, Ser92, Cys93, and Arg96) involved in interaction with Bim located in the vicinity of binding region were observed more stable.

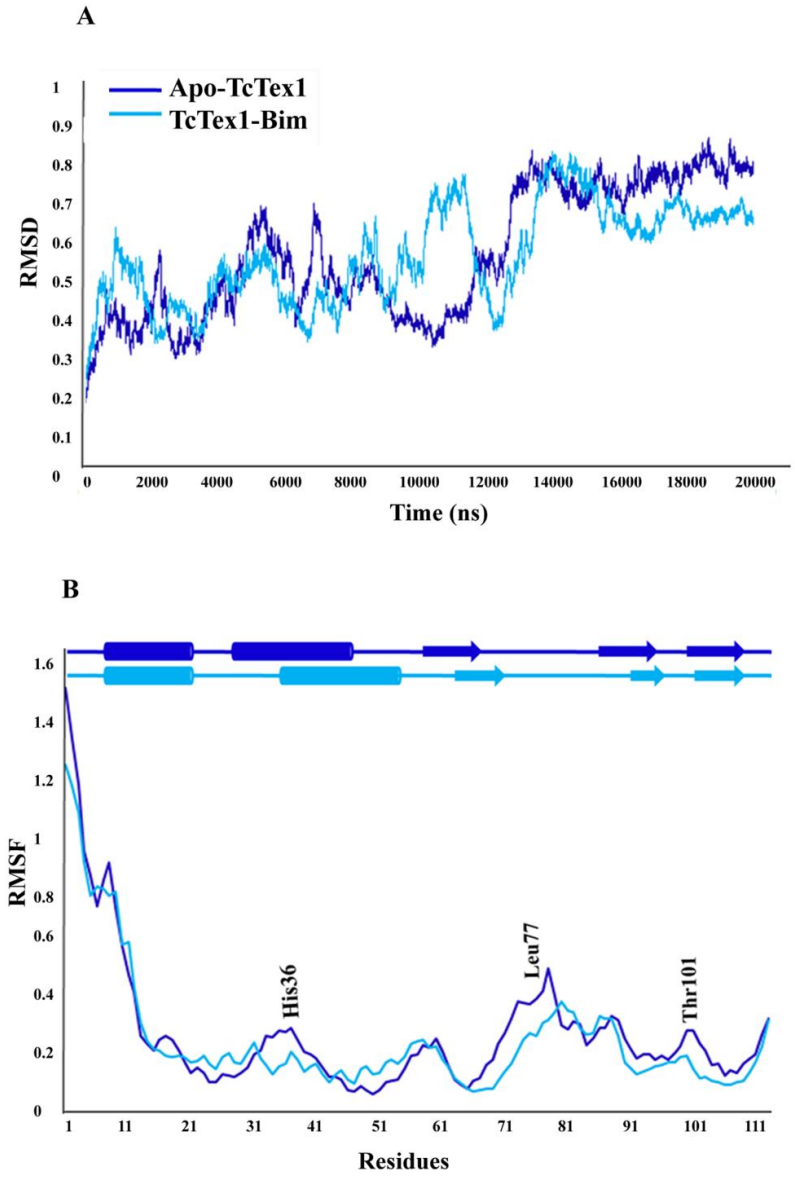

Figure 3.9: RMSF and RMSD plots of MD simulations for Tctex1. RMSF and RMSD plots are shown to examine fluctuation and stability of apo and bound-states of Tctex1. **(A)** Apo-Tctex1 and bound Tctex1 with Bim (Tctex1-Bim) are illustrated in blue and cyan colors, respectively. RMSD plot calculations are based on least square fitting of Cα-atoms. **(B)** RMSF plot showed fluctuations in comparison to apo-Tctex1.Secondary structure is demonstrated on the top. Arrows indicate β-strands, cylindrical shapes

describe α-helices and lines represent loop regions. Most fluctuated residues are labeled in black.

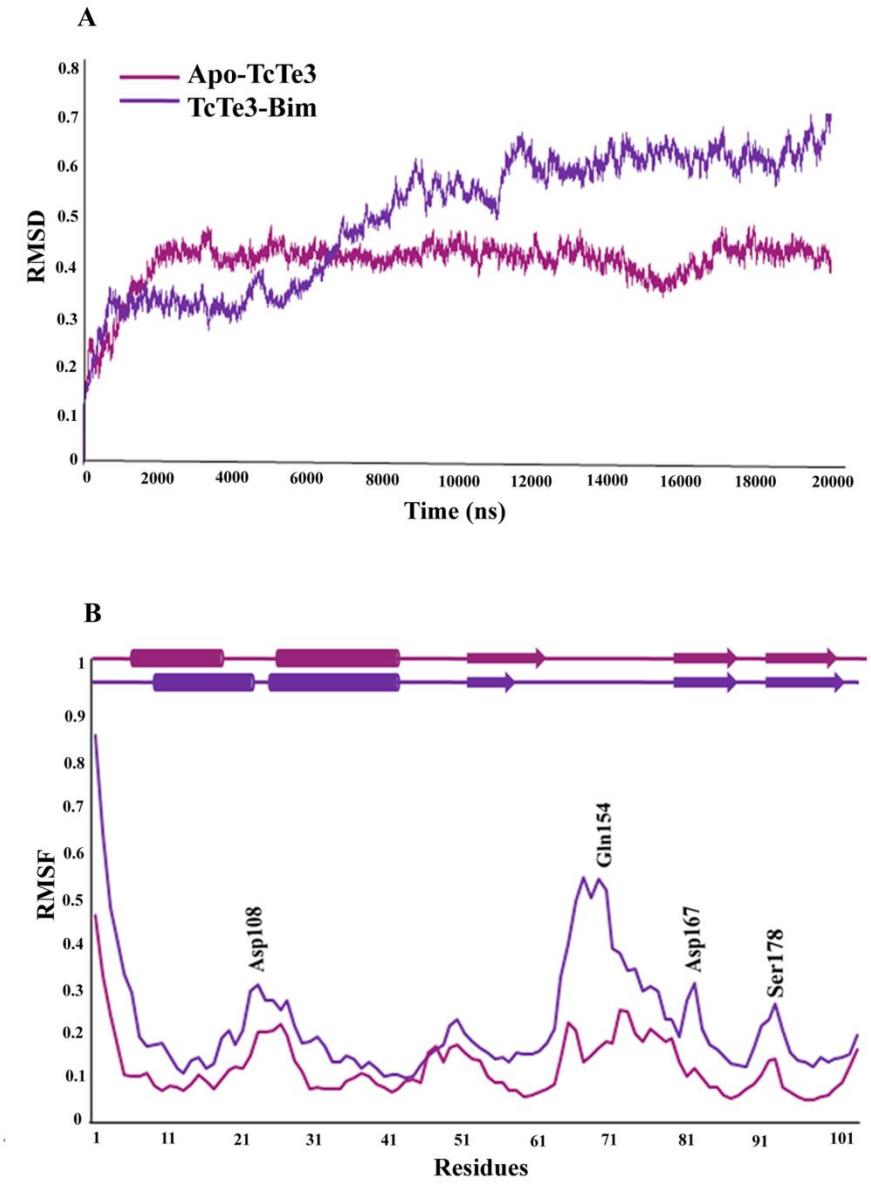

Figure 3.10: RMSD and RMSF plots of MD simulations for Tcte3. RMSD and RMSF plots (20ns) to scrutinize fluctuation and stability of apo and bound-states of Tcte3. **(A)** Apo-Tcte3 and bound Tcte3 with Bim (Tcte3-Bim) are illustrated in purple and magenta colors, respectively. RMSD plot calculations are based on least square fitting of C-alpha atoms. **(B)** RMSF plot showed fluctuations in comparison to apo-Tcte3 (magenta) and

Tcte3-Bim (purple). Secondary structure is demonstrated on the top. Arrows indicate β-strands, cylindrical shapes describe α-helices and lines represent loop regions. Most fluctuated residues are labeled in black.

3.6.3 Root mean square fluctuation analysis of Tcte3

In Tcte3-Bim complex, key fluctuations were pragmatic in Asp-108 (0.3071 Å), Gln152-Ile154 (0.5428-0.5406 Å), Asp167 (0.3076 Å) and Ser178 (0.2624 Å) residues (Figure 3.8B). The Tcte3 residues (Lys87, Leu145, Phe146, Ile147, Ile154, Asn155, Ile156, Ser158, Trp160, Ile161, Trp162, Asp163, Trp166, Asp167, Trp169, Leu182 and Phe186) were involved in Bim interaction revealed lesser fluctuations. These lesser fluctuations manifested more stability with a marked task in interaction. All conserved residues of Tcte3 (Leu87, Asn155, Ile156, Trp160 and Trp169) involved in interaction with Bim were stable, except Asp167 (0.3076Å). RMSF plot for Tcte3 indicated residual fluctuations in the loop regions, while comparatively no fluctuation was observed in the β-sheets and α-helical regions of Tcte3. Major fluctuations were observed in the loop regions of Tcte3 and Tctex1 (Figures 3.9 and 3.10).

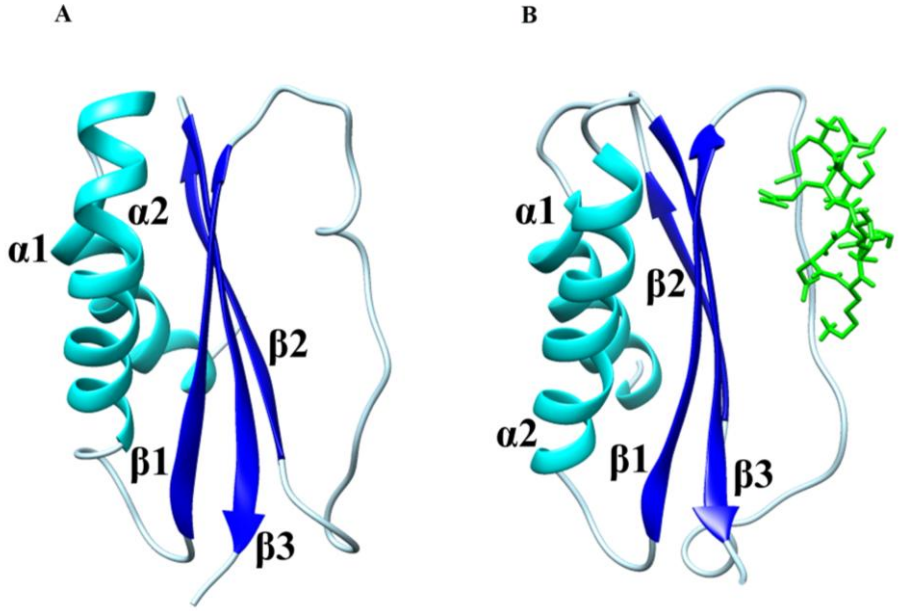

Figure 3.11: Secondary structuture analysis of Tctex1. It is focusing on conformational changes of apo-Tctex1 and Tctex1-Bim. **(A)** Apo-Tctex1 and **(B)** bound

Tctex1 with Bim illustrated the changes in secondary structures at 5 and 18ns. At 18ns, shrinkedα-helix of Tctex1 is observed. Extension of β-sheetin bound Tctex1 is also visible as compared to apo-Tctex1 (5ns). Secondary structures, α-helices, β-sheets and coils are represented in cyan, blue and light blue colors. Secondary structures are labeled in black color.

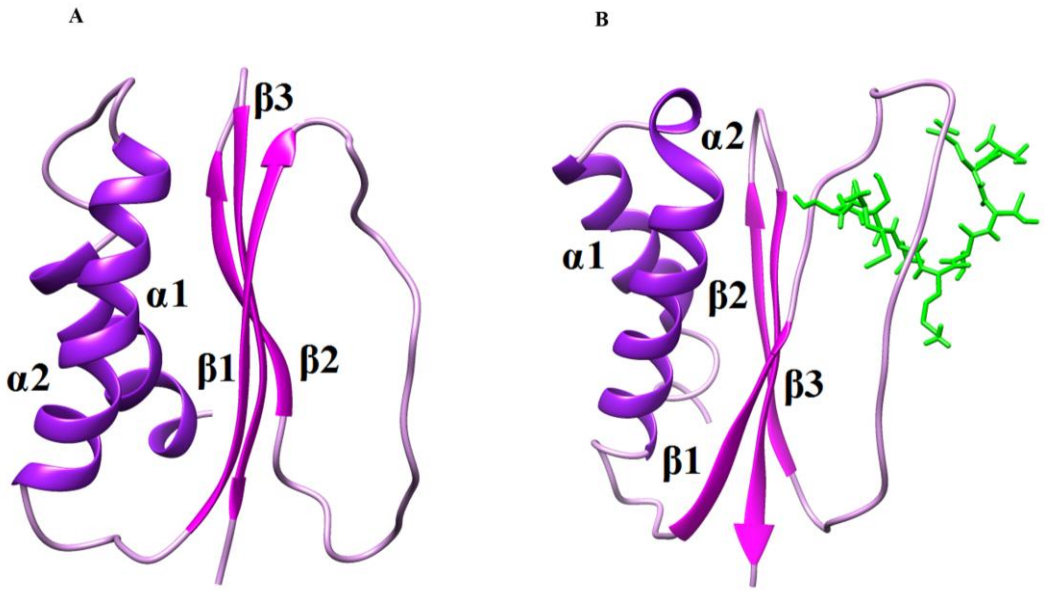

Figure 3.12: Conformational analysis of apo-Tcte3 and bound Tcte3-Bim. (A) Apo-Tcte3 at 1ns and **(B)** Tcte3-Bim at 18ns, bound state of Tcte3 with Bim (green) represented secondary structural changes against apo-Tcte3. β-sheets (magenta), α-helices (purple), loops (plum) and lables of secondary structure in black color.

3.6.4 Conformational Changes in Tctex1 and Tcte3

In comparative structural analysis between apo-Tctex1 and Tctex1-Bim at 18ns, major conformational changes were considered as extension of apo-Tctex1 loop2 region (Gly30- Gln-35) to three residues (Gly30-Lys38) (Figure 3.11). The α2 region (His36-Leu54) of apo-Tcte3 shifted to residual range (Val39- Lys56) in Tctex1-Bim. In case of Tcte3-Bim complex, main changes were following: apo-Tcte3 loop1 region (Leu86-Ala91) extended to Leu86-Thr96. The α1 (His92-Ser105) in apo-Tcte3 drifted towards the α1 (Lys97-Asp108) with respect to Tcte3-Bim complex (Figure 3.12). Loop2

(Val109- Lys110) was shrinked with respect to apo-Tcte3 loop2 (Leu106- Lys114). The α2 (Ala115- Glu132) in free state of Tcte3 shifted by 4 residues with reference to Tcte3-Bim α2 (Tyr111-Val130). β1 (Lys139-Val144) was shifted to Phe140-Gln148 as compared to apo-Tcte3.

4. DISCUSSION

Cell apoptosis is a complicated process which is influenced by various biochemical factors such as hormone level and pathway-specific apoptotic factors (Chausiaux *et al.,* 2008; Ruwanpura *et al.,* 2008). Cell death plays an essential function in multicellular organisms throughout their early development in sculpting the body organs by scheming cell homeostasis (Saikummar *et al.,* 1999). Apoptosis protects the organism by eliminating the cells injured by disease, infection, genetic mutation, aging and exposure to toxic agents (Wyllie *et al.,* 1980). Apoptosis has been recognized as a main feature that contributes to male infertility as it is necessary for usual spermatogenesis in mammals. A sufficient amount of germ cells is removed through apoptosis to maintain a particular germ cell population (Vaithinathan *et al.,* 2012).

Tctex1 (Tctex1 domain containing 1) and Tctex2/Tcte3 (t-complex-associated testis expressed 3) are germ cell-specific proteins that are expressed in testis and sperm. These proteins play an important role in male germ cell development (Ha *et al.,*1991; Huw *et al.,* 1995; Harrison *et al.,* 1998). Tcte3 and Tctex1 proteins exhibit high structural similarity to LC8 (PDB ID: 1F95). The LC8 monomer subunit comprises a small N-terminal strand followed by two helices (α1, α2). These helices are jam-packed against a 5-stranded β-sheet formed by one N-terminal strand and 4 other strands, one of which is consequent from the neighboring monomer. Two well-organized monomers form a symmetrical dimer (Kausar *et al.,*2013). We observed that Tctex1, Tcte3 and LC8 are structurally more conserved than at sequential level. Tctex1 and Tcte3 have the same structural topology as LC8 except the differences in β-sheets. The Tctex1 and Tcte3 β-sheets were more extended than that of LC8 β-sheets. Possibly, Tctex1 and Tcte3 may exist in dimer form in a similar way to that of LC8.The two LC8 monomers form a dimer through interactions between β2-strands of both monomers (Fan *et al.,* 2001). We elucidated the dimer formation of Tctex1 and Tcte3 by docking analysis. In both cases, the orientation was similar to LC8 dimer. It was demonstrated that homodimerization of all three dynein light chains (LC8, Tctex1 and Tcte3) resulted the two binding grooves at dimer interface where ligands can accommodate, while overall topology of homodimers was preserved in all three proteins. We scrutinized the dimerization interface by the

association of Bim (BH3-only protein) peptide at the binding groove. LC8 interacts with multiple viral and cellular proteins through its small consensus motif (K/R)XTQT. In LC8 targeted proteins, presence of two conserved consensus sequence motifs (K/R)XTQT and G(I/V)QV(D/E) is evident (Jaffrey and Snyder, 1996; Rodriguez-Crespo *et al.,* 2001; Lo *et al.,* 2001).

Tcte3 and Tctex1 are known to interact with LC8 and its target proteins (Lo *et al.,* 2001; Mok *et al.,* 2001; Williams *et al.,* 2005). Among them, a pro-apoptotic protein Bim has been reported to interact with LC8 that contains only 9 residues (MSCD**KSTQT**) (Puthalakath *et al.,* 1999; Fan *et al.,* 2001). LC8 binding groove for Bim involves β2-L4-β3 region. The Bim binding groove is generated between the two monomers by incorporating β1, β3 and mainly loop region which is evolved from β2-strand of LC8. Due to high structural similarity in Tctex1, Tcte3 and LC8, it was observed that through dimerization,Tctex1 and Tcte3 formed a similar groove to that of LC8 for binding to Bim. Predominantly, hydrophobic residues of loop and β-strand regions were involved in the formation of hydrophobic surface for Bim binding. We also performed molecular dynamics of apo-Tctex1, apo-Tcte3 and their complexes with Bim. The analysis indicated an overall stable binding profile for all systems which suggested that interactions of Tctex1 and Tcte3 with Bim were present in the vicinity of binding grooves.

Recent studies argue the role of Dynein light chains (DLCs) in apoptotic induction by linking the compartmentalization of pro-apoptotic cargoes (Puthalakath *et al.,*2004; Izidoro-Toledo *et al.,* 2013). It is a well-known fact that sequestering of Bcl-2 family proapoptotic protein Bim to microtubule-associated dynein motor complex is mediated by LC8 (Puthalakath *et al.,* 1999). Upon apoptotic stimuli, LC8 binding with dynein motor complex is disrupted and free LC8 interacts with Bim to neutralize the anti-apoptotic activity of Bcl-2.

Under normal conditions, LC8-Bim complex sequesters Bim to the microtubule-associated dynein complex. Upon apoptotic stimulation, LC8-Bim complex is released from the microtubule resulting in the dissociation of Bim that is free to neutralize the

anti-apoptotic activity of Bcl-2 by forming a Bim/Bcl-2 heterodimer (Puthalakath *et al.*,1999). It has been demonstrated that MEFs (mouse embryonic fibroblasts) lacking Bim/Bmf or Bax/Bak complexes are less susceptible to cell death than wild-type MEFs, suggesting the requirement of pro-apoptotic proteins as mediators of intrinsic apoptotic pathway in the absence of caspases (Gavathiotis *et al.,* 2008). Tctex1 and Tcte3 may transduce apoptotic signals to mitochondria by interacting with Bim in a similar manner to that of LC8 (Luo *et al.,* 2013). Phosphorylation of Bim by Pak1 (p21-activated kinase-1) may result in their dissociation from Tctex1 family (Tctex1 and Tcte3)and subsequent degradation by ubiquitin-proteasome. In the absence of free Bim, MAPK8/JNK (Mitogen-Activated protein kinase-8/c-Jun N-terminal kinase) is unable to phosphorylate and inhibit downstream signaling events to neutralize the anti-apoptotic Bcl-2 protein in mitochondria thus promoting cell survival. In response to apoptotic stimuli, Bim dissociates from Tctex1 family and free apoptotic proteins are phosphorylated by JNK/MAPK8. Through phosphorylation, stable Bim translocates to the mitochondria and activates other apoptotic facilitators like Bax, Bad and Bak to neutralize the effect of anti-apoptotic proteins like Bcl-2 and promote release of cytochrome-c thereby triggering the apoptosis via mitochondria-mediated pathway.

Conclusively, our detailed analysis investigated the sequence and structural similarities with LC8. We analyzed homodimerization of Tctex1 and Tcte3 by identifying binding grooves that might play an important role in interaction with Bim pro-apoptotic facilitator. We proposed common binding partner Bim for Tctex1 and Tcte3 which is involved in apoptosis by exploring similar mode of interaction to LC8. Our *in-silico* analysis explored the role of Tctex1 and Tcte3 in apoptosis on the basis of structural similarity and functional relevance with LC8.

In future, we aim to perform further computational approaches to investigate binding of dynein light chains Tctex1 and Tcte3 with Bim and dynein intermediate chains to explore the role of whole dynein complex In apoptotic pathway.

5. References

Abraham, M. J., & Gready, J. E. (2011). Optimization of parameters for molecular dynamics simulation using smooth particle-mesh Ewald in GROMACS 4.5. *Journal of computational chemistry*, 32(9), 2031-2040.

Adams, J. M., & Cory, S. (1998). The Bcl-2 protein family: arbiters of cell survival. *Science*, *281*(5381), 1322-1326.

Alberts, B. J. (2002). Alexander; Lewis, Julian; Raff, Martin; Roberts, Keith; Walter, Peter. *Molecular biology of the cell*, *4*, 1096-1102.

Altschul, S. F., Gish, W., Miller, W., Myers, E. W., & Lipman, D. J. (1990). Basic local alignment search tool. *Journal of molecular biology*, *215*(3), 403-410.

Altschul, S. F., Madden, T. L., Schäffer, A. A., Zhang, J., Zhang, Z., Miller, W., & Lipman, D. J. (1997). Gapped BLAST and PSI-BLAST: a new generation of protein database search programs. *Nucleic acids research*, *25*(17), 3389-3402.

ASAI, D. J., & WILKES, D. E. (2004). The dynein heavy chain family. *Journal of Eukaryotic Microbiology*, *51*(1), 23-29.

Baas, P. W., & Ahmad, F. J. (2001). Force generation by cytoskeletal motor proteins as a regulator of axonal elongation and retraction. *Trends in cell biology*, *11*(6), 244-249.

Barbar, E. (2008). Dynein light chain LC8 is a dimerization hub essential in diverse protein 8j networks. *Biochemistry*, *47*(2), 503-508.

Benashski, S. E., Harrison, A., Patel-King, R. S., & King, S. M. (1997). Dimerization of the highly conserved light chain shared by dynein and myosin V. *Journal of Biological Chemistry*, 272(33), 20929-20935.

Benison, G., Karplus, P. A., & Barbar, E. (2007). Structure and dynamics of LC8 complexes with KXTQT-motif peptides: swallow and dynein intermediate chain compete for a common site. *Journal of molecular biology*, *371*(2), 457-468.

Boutet, E., Lieberherr, D., Tognolli, M., Schneider, M., Bansal, P., Bridge, A. J., ...& Xenarios, I. (2016). UniProtKB/Swiss-Prot, the manually annotated section of the UniProtKnowledgeBase: how to use the entry view. *Plant bioinformatics: methods and protocols*, 23-54.

Bowman, A. B., Patel-King, R. S., Benashski, S. E., McCaffery, J. M., Goldstein, L. S., & King, S. M. (1999). Drosophila roadblock and Chlamydomonas LC7. *The Journal of cell biology*, *146*(1), 165-180.

Chausiaux, O. E., Abel, M. H., Baxter, F. O., Khaled, W. T., Ellis, P. J., Charlton, H. M., &Affara, N. A. (2008). Hypogonadal mouse, a model to study the effects of the endogenous lack of gonadotropins on apoptosis. *Biology of reproduction*, 78(1), 77-90.

Chen, V. B., Arendall, W. B., Headd, J. J., Keedy, D. A., Immormino, R. M., Kapral, G. J., ... & Richardson, D. C. (2010). MolProbity: all-atom structure validation for macromolecular crystallography. *ActaCrystallographica Section D: Biological Crystallography*, *66*(1), 12-21.

Chevalier-Larsen, E., &Holzbaur, E. L. (2006). Axonal transport and neurodegenerative disease. *BiochimicaetBiophysicaActa (BBA)-Molecular Basis of Disease*, 1762(11), 1094-1108.

Chuang, J. Z., Yeh, T. Y., Bollati, F., Conde, C., Canavosio, F., Caceres, A., & Sung, C. H. (2005). The dynein light chain Tctex-1 has a dynein-independent role in actin remodeling during neurite outgrowth. *Developmental cell*, *9*(1), 75-86.

Colovos, C., &Yeates, T. O. (1993). Verification of protein structures: patterns of nonbonded atomic interactions. *Protein science*, *2*(9), 1511-1519.

Conradt, B., & Horvitz, H. R. (1998). The C. elegans protein EGL-1 is required for programmed cell death and interacts with the Bcl-2–like protein CED-9. *Cell*, *93*(4), 519-529.

De Vries, S. J., Van Dijk, M., & Bonvin, A. M. (2010). The HADDOCK web server for data-driven biomolecular docking. *Nature protocols*, *5*(5), 883.

deVries, S. J., &Bonvin, A. M. (2011). CPORT: a consensus interface predictor and its performance in prediction-driven docking with HADDOCK. *PloS one*, *6*(3), e17695.

DiBella, L. M., Benashski, S. E., Tedford, H. W., Harrison, A., Patel-King, R. S., & King, S. M. (2001). The Tctex1/Tctex2 class of dynein light chains dimerization, differential expression, and interaction with the LC8 protein family. *Journal of Biological Chemistry*, 276(17), 14366-14373.

Doxsey, S. J., Stein, P., Evans, L., Calarco, P. D., &Kirschner, M. (1994). Pericentrin, a highly conserved centrosome protein involved in microtubule organization. *Cell*, *76*(4), 639-650.

Duan, Y., Wu, C., Chowdhury, S., Lee, M. C., Xiong, G., Zhang, W., ...& Caldwell, J. (2003). A point-charge force field for molecular mechanics simulations of proteins based on condensed-phase quantum mechanical calculations. *Journal of computational chemistry*, *24*(16), 1999-2012.

Dunker, A. K., Cortese, M. S., Romero, P., Iakoucheva, L. M., and Uversky, V. N. (2005) Flexible nets. The roles of intrinsic disorder in protein interaction networks, *FEBS Journal*,272, 5129 5148.

Eisenberg, D., Lüthy, R., & Bowie, J. U. (1997). [20] VERIFY3D: Assessment of protein models with three-dimensional profiles. *Methods in enzymology*, *277*, 396-404.

Elmore, S. (2007). Apoptosis: a review of programmed cell death. *Toxicologic pathology*, 35(4), 495-516.

Emsley, P., Lohkamp, B., Scott, W. G., &Cowtan, K. (2010). Features and development of Coot. *ActaCrystallographica Section D: Biological Crystallography*, *66*(4), 486-501.

Eswar, N., Eramian, D., Webb, B., Shen, M. Y., &Sali, A. (2008). Protein structure modeling with MODELLER. *Structural proteomics: high-throughput methods*, 145-159.

Eswar, N., John, B., Mirkovic, N., Fiser, A., Ilyin, V. A., Pieper, U., ...&Sali, A. (2003). Tools for comparative protein structure modeling and analysis. *Nucleic acids research*, 31(13), 3375-3380.

Fan, J. S., Zhang, Q., Tochio, H., Li, M., & Zhang, M. (2001). Structural basis of diverse sequence-dependent target recognition by the 8 kDa dynein light chain. *Journal of molecular biology*, 306(1), 97-108.

Frisch, S. M., &Screaton, R. A. (2001). Anoikis mechanisms. *Current opinion in cell biology*, 13(5), 555-562.

Gavathiotis, E., Suzuki, M., Davis, M. L., Pitter, K., Bird, G. H., Katz, S. G., ...& Walensky, L. D. (2008). BAX activation is initiated at a novel interaction site. *Nature*, 455(7216), 1076-1081.

Gibrat, J. F., Madej, T., & Bryant, S. H. (1996). Surprising similarities in structure comparison. *Current opinion in structural biology*, *6*(3), 377-385.

Gittes, F., Mickey, B., Nettleton, J., & Howard, J. (1993). Flexural rigidity of microtubules and actin filaments measured from thermal fluctuations in shape. The Journal of cell biology, 120(4), 923-934.

Goode, B. L., Drubin, D. G., & Barnes, G. (2000). Functional cooperation between the microtubule and actin cytoskeletons. *Current opinion in cell biology*, *12*(1), 63-71.

Ha, H., Howard, C. A., Yeom, Y. I., Abe, K., Uehara, H., Artzt, K., & Bennett, D. (1991). Several testis-expressed genes in the mouse t-complex have expression differences between wild-type and t-mutant mice. *Genesis*, 12(4), 318-332.

Ha, J., Lo, K. W. H., Myers, K. R., Carr, T. M., Humsi, M. K., Rasoul, B. A., ...&Pfister, K. K. (2008). A neuron-specific cytoplasmic dynein isoform preferentially transports TrkB signaling endosomes. *The Journal of cell biology*, 181(6), 1027-1039.

Harrison, A., Olds-Clarke, P., & King, S. M. (1998). Identification of the t complex–encoded cytoplasmic dynein light chain Tctex1 in inner arm I1 supports the involvement of flagellardyneins in meiotic drive. *The Journal of cell biology*, 140(5), 1137-1147.

Hirokawa, N., & Noda, Y. (2008). Intracellular transport and kinesin superfamily proteins, KIFs: structure, function, and dynamics. *Physiological reviews*, 88(3), 1089-1118.

Hirokawa, N., Noda, Y., Tanaka, Y., &Niwa, S. (2009). Kinesin superfamily motor proteins and intracellular transport. *Nature reviews Molecular cell biology*, 10(10), 682-696.

Hughes, S. M., Vaughan, K. T., Herskovits, J. S., &Vallee, R. B. (1995). Molecular analysis of a cytoplasmic dynein light intermediate chain reveals homology to a family of ATPases. *Journal of Cell Science*, 108(1), 17-24.

Huw, L. Y., Goldsborough, A. S., Willison, K., &Artzt, K. (1995). Tctex2: a sperm tail surface protein mapping to the t-complex. *Developmental biology*, 170(1), 183-194.

Ishikawa, T. (2012). Structural biology of cytoplasmic and axonemal dyneins. *Journal of structural biology*, 179(2), 229-234.

Izidoro-Toledo, T. C., Borges, A. C., Araújo, D. D., Mazzi, D. L., Nascimento, F. O., Sousa, J. F., ... & Peixoto, P. M. (2013). A myosin-Va tail fragment sequesters dynein light chains leading to apoptosis in melanoma cells. *Cell death & disease*, 4(3), e547.

Jaffrey, S. R., & Snyder, S. H. (1996). PIN: an associated protein inhibitor of neuronal nitric oxide synthase. *Science*, 274(5288), 774.

Kausar, S., Asif, M., Bibi, N., & Rashid, S. (2013). Comparative molecular docking analysis of cytoplasmic dynein light chain DYNLL1 with pilin to explore the molecular mechanism of pathogenesis caused by Pseudomonas aeruginosa PAO. *PloS one*, *8*(10), e76730.

Kelekar, A., & Thompson, C. B. (1998). Bcl-2-family proteins: the role of the BH3 domain in apoptosis. *Trends in cell biology*, 8(8), 324-330.

King, S. M. (2012). Integrated control of axonemal dynein AAA+ motors. *Journal of structural biology*, 179(2), 222-228.

King, S. M., Barbarese, E., Dillman, J. F., Patel-King, R. S., Carson, J. H., & Pfister, K. K. (1996). Brain cytoplasmic and flagellar outer arm dyneins share a highly conserved Mr 8,000 light chain. *Journal of Biological Chemistry*, 271(32), 19358-19366.

Kozakov, D., Beglov, D., Bohnuud, T., Mottarella, S. E., Xia, B., Hall, D. R., & Vajda, S. (2013). How good is automated protein docking?. *Proteins: Structure, Function, and Bioinformatics*, 81(12), 2159-2166.

Kuta, A., Deng, W., El-Kadi, A. M., Banks, G. T., Hafezparast, M., Pfister, K. K., & Fisher, E. M. (2010). Mouse cytoplasmic dynein intermediate chains: identification of new isoforms, alternative splicing and tissue distribution of transcripts. *PloS one*, 5(7), e11682.

Lacy, E. R., Wang, Y., Post, J., Nourse, A., Webb, W., Mapelli, M., ...& Kriwacki, R. W. (2005). Molecular basis for the specificity of p27 toward cyclin-dependent kinases that regulate cell division. *Journal of molecular biology*, 349(4), 764-773.

Li, W., Cowley, A., Uludag, M., Gur, T., McWilliam, H., Squizzato, S., ...& Lopez, R. (2015). The EMBL-EBI bioinformatics web and programmatic tools framework. *Nucleic acids research*, 43(W1), W580-W584.

Liang, J., Jaffrey, S. R., Guo, W., Snyder, S. H., & Clardy, J. (1999). Structure of the PIN/LC8 dimer with a bound peptide. *Nature structural biology*, 6(8).

Lo, K. W. H., Kan, H. M., &Pfister, K. K. (2006). Identification of a novel region of the cytoplasmic Dynein intermediate chain important for dimerization in the absence of the light chains. *Journal of Biological Chemistry*, 281(14), 9552-9559.

Lo, K. W. H., Kogoy, J. M., &Pfister, K. K. (2007). The DYNLT3 light chain directly links cytoplasmic dynein to a spindle checkpoint protein, Bub3. *Journal of Biological Chemistry*, 282(15), 11205-11212.

Lo, K. W. H., Naisbitt, S., Fan, J. S., Sheng, M., & Zhang, M. (2001). The 8-kDa dynein light chain binds to its targets via a conserved (K/R) XTQT motif. *Journal of Biological Chemistry*, 276(17), 14059-14066.

Lohkamp, B., Emsley, P., & Cowtan, K. (2005). Coot news. *CCP4 Newsletter*, 42, 3-5.

Lovell, S. C., Davis, I. W., Arendall, W. B., de Bakker, P. I., Word, J. M., Prisant, M. G., ... & Richardson, D. C. (2003). Structure validation by Cα geometry: ϕ, ψ and Cβ deviation. Proteins: Structure, Function, and Bioinformatics, 50(3), 437-450.

Luo, S., & Rubinsztein, D. C. (2013). BCL2L11/BIM: a novel molecular link between autophagy and apoptosis. *Autophagy*, 9(1), 104-105.

Ma, S., Triviños-Lagos, L., Gräf, R., & Chisholm, R. L. (1999). Dynein Intermediate Chain Mediated Dynein–Dynactin Interaction Is Required for Interphase Microtubule Organization and Centrosome Replication and Separation in Dictyostelium. *The Journal of cell biology*, 147(6), 1261-1274.

Makokha, M., Hare, M., Li, M., Hays, T., &Barbar, E. (2002). Interactions of cytoplasmic dynein light chains Tctex-1 and LC8 with the intermediate chain IC74. *Biochemistry*, 41(13), 4302-4311.

McKenney, R. J., Huynh, W., Tanenbaum, M. E., Bhabha, G., & Vale, R. D. (2014). Activation of cytoplasmic dynein motility by dynactin-cargo adapter complexes. *Science*, 345(6194), 337-341.

Mok, Y. K., Lo, K. W. H., & Zhang, M. (2001). Structure of Tctex-1 and its interaction with cytoplasmic dynein intermediate chain. *Journal of Biological Chemistry*, 276(17), 14067-14074.

Morris, G. M., Huey, R., Lindstrom, W., Sanner, M. F., Belew, R. K., Goodsell, D. S., & Olson, A. J. (2009). AutoDock4 and AutoDockTools4: Automated docking with selective receptor flexibility. *Journal of computational chemistry*, 30(16), 2785-2791.

Navarro-Lérida, I., Martínez Moreno, M., Roncal, F., Gavilanes, F., Albar, J. P., & Rodríguez-Crespo, I. (2004). Proteomic identification of brain proteins that interact with dynein light chain LC8. *Proteomics*, 4(2), 339-346.

Neesen, J., Drenckhahn, J. D., Tiede, S., Burfeind, P., Grzmil, M., Konietzko, J., ...& Omran, H. (2002). Identification of the human ortholog of the t-complex-encoded protein TCTE3 and evaluation as a candidate gene for primary ciliary dyskinesia. *Cytogenetic and genome research*, 98(1), 38-44.

Neuwald, A. F., Aravind, L., Spouge, J. L., &Koonin, E. V. (1999). AAA+: A class of chaperone-like ATPases associated with the assembly, operation, and disassembly of protein complexes. *Genome research*, 9(1), 27-43.

Oltval, Z. N., Milliman, C. L., &Korsmeyer, S. J. (1993). Bcl-2 heterodimerizes in vivo with a conserved homolog, Bax, that accelerates programed cell death. *Cell*, 74(4), 609-619.

Paschal, B. M., King, S. M., Moss, A. G., Collins, C. A., Vallee, R. B., & Witman, G. B. (1987). Isolated flagellar outer arm dynein translocates brain microtubules in vitro. *Nature*, 330(6149), 672-674.

Pettersen, E. F., Goddard, T. D., Huang, C. C., Couch, G. S., Greenblatt, D. M., Meng, E. C., & Ferrin, T. E. (2004). UCSF Chimera—a visualization system for exploratory research and analysis. *Journal of computational chemistry*, *25*(13), 1605-1612.

Pfister, K. K., Shah, P. R., Hummerich, H., Russ, A., Cotton, J., Annuar, A. A., ... & Fisher, E. M. (2006). Genetic analysis of the cytoplasmic dynein subunit families. *PLoS genetics*, 2(1), e1.

Phizicky, E., Bastiaens, P. I., Zhu, H., Snyder, M., & Fields, S. (2003). Protein analysis on a proteomic scale. *Nature*, 422(6928), 208-215.

Purohit, A., Tynan, S. H., Vallee, R., &Doxsey, S. J. (1999). Direct interaction of pericentrin with cytoplasmic dynein light intermediate chain contributes to mitotic spindle organization. *The Journal of cell biology*, 147(3), 481-492.

Puthalakath, H., Gretchen, S. K. E. A., Strasser, A., Barsukov, I., Lu-Yun, L. I. A. N., Huang, D. C., & Hinds, M. G. (2004). Localization of dynein light chains 1 and 2 and their pro-apoptotic ligands. *Biochemical Journal*, 377(3), 597-605.

Puthalakath, H., Huang, D. C., O'Reilly, L. A., King, S. M., &Strasser, A. (1999). The proapoptotic activity of the Bcl-2 family member Bim is regulated by interaction with the dynein motor complex. *Molecular cell*, 3(3), 287-296.

Rapali, P., Szenes, A., Radnai, L., Bakos, A., Pal, G., &Nyitray, L. (2011). DYNLL/LC8: a light chain subunit of the dynein motor complex and beyond. *The FEBS journal*, 278(17), 2980-2996.

Rayan, A. (2009). New tips for structure prediction by comparative modeling. *Bioinformation*, *3*(6), 263.

Roberts, A. J., Kon, T., Knight, P. J., Sutoh, K., & Burgess, S. A. (2013). Functions and mechanics of dynein motor proteins. *Nature reviews Molecular cell biology*, *14*(11), 713-726.

Rodríguez-Crespo, I., Yélamos, B., Roncal, F., Albar, J. P., Ortiz de Montellano, P. R., & Gavilanes, F. (2001). Identification of novel cellular proteins that bind to the LC8 dynein light chain using a pepscan technique. *FEBS letters*, 503(2-3), 135-141.

Ruwanpura, S. M., McLachlan, R. I., Stanton, P. G., Loveland, K. L., & Meachem, S. J. (2008). Pathways involved in testicular germ cell apoptosis in immature rats after FSH suppression. *Journal of Endocrinology*, 197(1), 35-43.

Saikumar, P., & Venkatachalam, M. A. (2009). Apoptosis and cell death. In *Basic Concepts of Molecular Pathology* (pp. 29-40). Springer US.

Saikumar, P., Dong, Z., Mikhailov, V., Denton, M., Weinberg, J. M., &Venkatachalam, M. A. (1999). Apoptosis: definition, mechanisms, and relevance to disease. *The American journal of medicine*, 107(5), 489-506.

Šali, A., & Blundell, T. L. (1993). Comparative protein modelling by satisfaction of spatial restraints. *Journal of molecular biology*, 234(3), 779-815.

Schrader, M., & Schulz-Knappe, P. (2001). Peptidomics technologies for human body fluids. *Trends in biotechnology*, 19(10), S55-S60.

Schroer, T. A. (2004). Dynactin. *Annual Review Cell Development Biology*, 20, 759-779.

Schumann-Gillett, A., Mark, A. E., Deplazes, E., & O'Mara, M. L. (2017). A potential new, stable state of the E-cadherin strand-swapped dimer in solution. *European Biophysics Journal*, 1-9.

Shen, M. Y., & Sali, A. (2006). Statistical potential for assessment and prediction of protein structures. *Protein science*, 15(11), 2507-2524.

Stelzl, U., Worm, U., Lalowski, M., Haenig, C., Brembeck, F. H., Goehler, H., ...& Timm, J. (2005). A human protein-protein interaction network: a resource for annotating the proteome. *Cell*, 122(6), 957-968.

Strasser, A., Cory, S., & Adams, J. M. (2011). Deciphering the rules of programmed cell death to improve therapy of cancer and other diseases. *The EMBO journal*, 30(18), 3667-3683.

Sussman, J. L., Lin, D., Jiang, J., Manning, N. O., Prilusky, J., Ritter, O., & Abola, E. E. (1998). Protein Data Bank (PDB): database of three-dimensional structural information of biological macromolecules. *ActaCrystallographica Section D: Biological Crystallography*, 54(6), 1078-1084.

Tai, A. W., Chuang, J. Z., Bode, C., Wolfrum, U., & Sung, C. H. (1999). Rhodopsin's carboxy-terminal cytoplasmic tail acts as a membrane receptor for cytoplasmic dynein by binding to the dynein light chain Tctex-1. *Cell*, 97(7), 877-887.

Thompson, R. F., & Langford, G. M. (2002). Myosin superfamily evolutionary history. The Anatomical Record, 268(3), 276-289.

Trott, O., & Olson, A. J. (2010). AutoDockVina: improving the speed and accuracy of docking with a new scoring function, efficient optimization, and multithreading. *Journal of computational chemistry*, 31(2), 455-461.

Tsujimoto, Y., & Shimizu, S. (2000). Bcl-2 family: life-or-death switch. *FEBS letters*, 466(1), 6-10.

Tsujimoto, Y., & Shimizu, S. (2000). VDAC regulation by the Bcl-2 family of proteins. *Cell death and differentiation*, 7(12), 1174.

Tynan, S. H., Purohit, A., Doxsey, S. J., &Vallee, R. B. (2000). Light intermediate chain 1 defines a functional subfraction of cytoplasmic dynein which binds to pericentrin. *Journal of Biological Chemistry*, 275(42), 32763-32768.

UniProt Consortium. (2008). The universal protein resource (UniProt). *Nucleic acids research*, 36(1), D190-D195.).

Vaithinathan, S., Saradha, B., &Mathur, P. P. (2010). Methoxychlor induces apoptosis via mitochondria-and FasL-mediated pathways in adult rat testis. *Chemico-biological interactions*, 185(2), 110-118.

Vale, R. D. (2003). The molecular motor toolbox for intracellular transport. *Cell*, 112(4), 467-480.

Wallace, A. C., Laskowski, R. A., & Thornton, J. M. (1995). LIGPLOT: a program to generate schematic diagrams of protein-ligand interactions. *Protein Engineering, Design and Selection*, 8(2), 127-134.

Wanschers, B., van de Vorstenbosch, R., Wijers, M., Wieringa, B., King, S. M., & Fransen, J. (2008). Rab6 family proteins interact with the dynein light chain protein DYNLRB1. *Cell motility and the cytoskeleton*, 65(3), 183-196.

Webb, B., & Sali, A. (2014). Protein structure modeling with MODELLER. *Protein Structure Prediction*, 1-15.

Wickstead, B., & Gull, K. (2007). Dyneins across eukaryotes: a comparative genomic analysis. *Traffic*, *8*(12), 1708-1721.

Wiederstein, M., & Sippl, M. J. (2007). ProSA-web: interactive web service for the recognition of errors in three-dimensional structures of proteins. *Nucleic acids research*, 35, W407-W410.

Williams, J. C., Xie, H., & Hendrickson, W. A. (2005). Crystal structure of dynein light chain TcTex-1. *Journal of Biological Chemistry*, 280(23), 21981-21986.

Wilson, M. J., Salata, M. W., Susalka, S. J., &Pfister, K. K. (2001). Light chains of mammalian cytoplasmic dynein: identification and characterization of a family of LC8 light chains. *Cytoskeleton*, 49(4), 229-240.

Workbench, C.G., v3. 6., 2010. Now new version can be available at <http://www. clcbio.com/products/clc genomics work bench

Wyllie, A. H., Kerr, J. R., & Currie, A. R. (1980). Cell death: the significance of apoptosis. *International review of cytology*, 68, 251-306.

Yuan, J. (1996). Evolutionary conservation of a genetic pathway of programmed cell death. *Journal of cellular biochemistry*, 60(1), 4-11.

thesis

by Sonia Kanwal

FILE	FOR_PLGRSM.DOCX (50.86K)		
TIME SUBMITTED	19-JUL-2017 05:25PM	WORD COUNT	7401
SUBMISSION ID	831914783	CHARACTER COUNT	42664

The major aim of current research is to identify the role of DLCs(TcTe3 and TcTex1) in programmed cell death. In order to perform these tasks, Three-dimensional structure prediction of humanTcTe3 and Tctex1 will be carried out. The structural comparison of DLCs will enable to isolate functional relevance in motor components. Comparative molecular interaction study of LC8, TcTe3 and TcTex1 with apoptotic facilitators will be carried out to explore the functional implications of these proteins in apoptosis. The interaction assay will be elaborated through molecular dynamics simulation assays.

members (Bax, Noxa and Puma) are transcriptionally activated based on DNA damage. During apoptosis, cytoplasmic Bid moves towards mitochondria followed by cleavage (Tisujimoto and Shimizu, 2000). Bim and Bmf act in response to that apoptotic signals transmitted by apoptotic signals. Bim is involved in binding with microtubular dynein motor complex by means of LC8, while Bmf connects to myosin V actin motor complex through interaction with DLC2. These proteins are translocated to mitochondria upon apoptotic stimuli (Tsujimoto and Sujimizu, 2000). Ultraviolet (UV) radiations appear to release Bim and Bmf. These BH3-only proteins act as intracellular apoptotic sensors which induce signals to mitochondria through pro-apoptotic BCL family members having multi domains (Frisch and Screato, 2001).

The role of motor complexes is to seize the pro-apoptotic 'BH3-only' (Bcl-2 homology 3-only) proteins, Bim (Bcl-2-interacting mediator of cell death) and Bmf (Bcl-2-modifying factor) during the regulation of apoptosis (Puthalakath *et al.,* 2004). DLC1 is a substrate of p21-activated kinase 1 (Pak1) which plays a vital role in cell survival based on phosphorylation process. Pak1 phosphorylates Bim and prevents it from further interaction which causes inactivation of BCL-2 (anti-apoptotic protein). BCL family

The BCL-2 family proteins are involved in apoptotic processes by acting as important gatekeepers. BCL family consists of structurally similar pro-apoptotic and anti-apoptotic proteins. BCL members must have at least one BH motif (Strasser *et al.,* 2011). BCL-2 family contains 15 members in mammalian cells and numerous others in viruses (Adams and Cory, 1998). All members have four conserved domains BH1 to BH4. Most anti-apoptotic members exhibit BH1 and BH2 motifs to inhibit apoptosis. The members closely related to BCL-2 have all four BH domains (BH1-BH4). The pro-apoptotic members (Bax, Bak, and Bok) are closely related to BCL-2 and contain BH1, BH2, BH3 domains. These subfamilies differ markedly in their relatedness to Bcl-2. Bax, Bak, and Bok contain BH1, BH2, and BH3domains. In comparison, 7 other mammalian pro-apoptotic members possess only 9 to 16 AA, named as BH3 domain (Kelekar and Thompson, 1998). The BH3 domain acts as functional antagonists of anti-

apoptotic proteins during programmed cell death (Conradt and Horvitz, 1998). BH3 is essential for pro-apoptotic proteins including C. elegance protein EGL-1 (Lelekar and Thompson, 1998). BCL family members (Pro- and anti-apoptotic) can heterodimerize and affect one another's function (Oltyal *et al.,* 1993).

of toxic agents (Saikumar and Venkatachalam, 2009). Apoptosis can be divided into three stages, commitment phase (extracellular or intracellular signals initiate cell death specifically), execution phase and cleanup phase (degradation in lysosomes of phagocytic cells and dead cells are removed) (Platt *et al.,* 1998). The apoptotic mechanism is conserved throughout evolution from worm to human (Yuan, 1996).

Apoptosis is a vital constituent of a variety of processes (Cell division, chemical-induced cell death, system, hormone-dependent atrophy, embryonic development, growth and functioning of the immune system. Aberrant apoptosis causes many abnormalities in human, neurodegenerative diseases, autoimmune disorders, ischemic damage and numerous kinds of cancer (Elmore, 2007). Cell death (apoptosis) plays a crucial role in eukaryotic organisms during embryonic development and cell division. Apoptosis prevents the organism by damaged cell, genetic mutation, aging, infection and disclosure

DYNLL proteins were originally identified as LC. The isoforms of LC8 family are motor proteins (microtubule-based) dynein (Benashski *et al.,* 1997). DYNLL proteins are evolutionary conserved (>94% sequence similarity between *Drosophila melanogaster* and mammals) (Wilson *et al.,* 2001). Mammals articulate two strongly related isoforms: DYNLL1 (LC8a, DLC1, or PIN) and DYNLL2 (LC8b or DLC2), respectively. DYNLL2 shows 93% identity with DYNLL1 (Pfister *et al.,* 2006).

LC8 interacts with proteins having K/RSTQT or GIQVD motifs to permit their transport in a retrospective way (Navarro Lérida *et al.,* 2004).These proteins are involved in different processes including apoptosis, kidney development, enzyme regulation and viral pathogenesis (Lacy *et al.,* 2005). LC8 is a hub protein that is essential for diverse protein networks (Dunker *et al.,* 2005). The central modulatory roles of LC8 are due to its capability to endorse dimerization (Barber, 2008). LC8 functions as a cargo adapter related with both motor and cargo protein (Fan *et al.,* 2001). LC8promotes structural stabilization and dimerization. LC8 controls binding of its partners in various protein complexes as dynein motor complex (Barber, 2008)

Dynein Light Roadblock (DYNLRB), a class of DLC has capability of modulating GTPase activity of GTP-binding proteins. Members of Roadblock family are structurally similar proteins. These proteins regulate small GTPases (Wanschers *et al.,* 2008).

The Tctex1(t-complex testis-expressed-1) family of LCs consists of two isoforms: Dynein Light chain 1 (DYNLT1) and Dynein Light chain 3 (DYNLT3). These two isoforms help dynein to connect with its specific cargoes. DYNLT3 is involved in transportation of checkpoint proteins between kinetochore and spindle pole. DYNLT3 is also important for congression of chromosome (Lo *et al.,* 2007).

Partial structural organization of TcTex1 depicts that TcTex1 may bind directly to IC at N-terminus. Tctex-1 exhibits structural similarities with LC8 despite lacking sequence similarity (Mok *et al.,* 2001). Tctex-1 is involved in axonal specification, neurite development and hippocampal neurons growth (Chuang *et al*, 2005). Tctex-1 acts as a component of inner arm. TcTex1 performs independent functions other than movements. Tctex-1 is profusely expressed in post-mitotic neurons at embryonic stages and plays vital role in neuritogenesis (Chuang *et al*, 2005). Tctex-1 expression restricts primarily to the Golgi apparatus in interphase fibroblasts (Tai *et al.*, 1999)

The human orthologous *TcTe3* gene was mapped on chromosome 6q27 (Neesen et al., 2002). TcTe3 encoded protein shares 87% homology. TcTe3 is mainly expressed during male germ cell development in brain, lung, and trachea tissues (DiBella *et al.,* 2001). The predominant expression of TcTe3 in somatic and male germ cells has detected by several recent studies (Huw *et al.,* 1995)

Cytoplasmic dynein contains a low molecular weight14-kDa light chain (LC) known as Tctex-1. LCs function by attaching specific cargoes to the dynein complex (King *et al.*, 1996; Bowman *et al.*, 1999; Tai *et al.*, 1999). In dynein complex, three classes of LCs are well-characterized.

Cytoplasmic dynein light intermediate chains (DLICs) have homology with transporter family (ABC) of ATPases. DLIC contains potential ATPase activity and acts as a novel family of dynein subunits. DLICs show complexity due to their post translational modification (Hughes *et al.*, 1995). LIC1 attaches to pericentrin (structural component of centrosome) involved in

microtubule association and function (Doxsey *et al.*, 1994; Purohit *et al.*, 1999), signifying that this subunit is implicated in connecting dynein to its cargo (Purohit *et al.*, 1999; Tynan *et al.*, 2000).

The intermediate chains DYNC1I1 (IC1) and DYNC1I2 (IC2) are involved in binding with cargo (Ha *et al.*, 2008). Interaction of dynein complex and cargo occurs in the presence of dynactin complex. Dynactin complex binds to dynein intermediate chains (DIC) to adapt dynein-cargo interactions. Dynactin complex also shows interaction with microtubule to regulate the dynein movement (Chevalier-Larsen and Holzbaur, 2006; Schroer, 2004). The intermediate chains (IC1 and IC2) are involved in direct binding with other protein cargos (beta-catenin, kinesin light chains 1 and 2, casein kinase II, huntingtin and neurofilament) (Kuta *et al.*, 2010). IC1 and IC2 possess 69% similarity and contain an approximate molecular weight of about 74 kDa (Paschal *et al.*, 1987).Intermediate chains form homo- or heterodimers (Lo *et al.*, 2006). DICs interact with dynactin through N-terminus, while its C-terminus is associated with heavy chains by means of WD40 (Ma et al., 1999).

dynein heavy chain is a massive structure (4600 residues). The length of dynein heavy chain is greater than twice the size of myosin II and mass of kinesin. Dynein heavy chain moves along microtubule in particular directions (Ishikawa, 2012). There is a great distinction in numeral of dynein heavy chain genes in eukaryotes (Vale, 2003).

Cytoplasmic dynein consists of heavy, intermediate, light intermediate and light chains which are involved in many biological processes (Figure 1.2). Cytoplasmic dynein (molecular mass of about 1.5 mega Daltons) is a complex of dimer which is composed of twelve polypeptides. Two identical heavy chains (520 kDa) regulate ATPase activity and mediate microtubule-dependent movement. The two intermediate chains (74 kDa), two light intermediate chains (53–59 kDa) and a number of light chains (McKenney *et al.*, 2014) help to attach dynein to its cargo. Cytoplasmic dynein performs enormous cellular functions (Wickstead and Gul, 2007). Cytoplasmic dynein members of mouse and human represented in table 1.1.

Axonemal dyneins exist in complex form by containing one, two or three non-identical heavy chains depending on organism and cilium location. Heavy chain is comprised of doughnut-shaped structure (globular motor domain) similar to AAA proteins, a twisting coil 'stalk'

(interacts with microtubule), and an elongated tail (stem) which binds to adjacent microtubule of similar axoneme (Karp, 2005). The regulated activity of axonemal dynein is significant for ciliary waveform and flagellar strike frequency. The regulation of axonemal dynein includes calcium mode, phosphorylation and redox activity (King, 2012).

Dynein is one of the cytoskeletal motor proteins that is essential for smooth movement of microtubules through the thrashing of cilia and flagella located on eukaryotic cell surfaces (Roberts *et al.,* 2013). Dynein belongs to superfamily AAA (ATPases related with assorted actions) (Neuwald *et al.,* 1999). Dyneins are divided into two groups: axonemal and cytoplasmic dyneins.

Kinesin generates the motile strength by driving conformational changes through the utilization of ATP hydrolysis (Hirokawa and Noda, 2008). Kinesin is a superfamily proteins, act as significant motor proteins for transportation of cargos. Kinesin is involved in the transportation of protein complexes, mRNAs and membrane bounded organelles. Recent studies suggest different mechanisms to recognize kinesin binding to specific cargos, unloading and adjusting the direction of movement. Recent *in- vivo* experiments have exposed imperative and unpredicted functions of kinesins in various physiological processes (developmental patterning, brain function and tumor repression) (Hirokawa *et al.,* 2009).

In essential cellular functions (vesicle trafficking and cell division), motor proteins utilize microtubules as substrates. Microtubules are involved in interaction with major motor proteins like kinesin (moves towards microtubule positive end) and dynein (moves towards negative end of microtubule) (Hirokawa *et al.,* 2009).

protein is composed of two heavy chains (motor head) and two light chains. Myosin head contains ATP and actin interaction sites. The movement towards plus (+) end of actin filament provides energy. In cell division, myosin II plays an essential role. Bipolar thick filaments of myosin II divide parent cell into two daughter cells by contraction force during cytokinesis. Myosin is also responsible for multiple non-muscle cells movement. At cell surface, myosin I is engaged in intracellular association and the projection of structures (actin-rich). Organelle and vesicle transport is proscribed by myosin V (Alberts, 2002). Myosin XI is involved in the

cytoplasmic streaming which allows organelles to stream along with microfilaments (Thompson and Langford, 2002).

Actin motors are connected in a manner to form hetero-motor complexes. The best example of such confirmation is 'myosin' (Goode *et al.*, 2000).

The movement of motor proteins is carried out in two ways on the basis of their substrates. Actin motors (myosin) follow the movement along microfilaments by considering actin interaction. Microtubule motors (kinesin and dynein) move with the help of microtubules through tubulin interaction. Cytoskeletal motor proteins are classified into two categories based on carrying movement direction along microtubules within cell i.e., plus-end motors: actin motors and minus-end motors: microtubule motors (Bass and Ahmad, 2001).

There are prominent similarities in these three cytoskeletal motors (myosin, kinesin, and dynein) as they are independently evolved and not homologues. Each motor protein converts chemical energy into mechanical energy by means of ATP hydrolysis (Howard, 2001). All motor proteins exist in complex form which consists of several components. The regulation of motor activity is mediated by heavy chain. The intermediate and light chains arbitrate the tethering of motor to molecular cargo. The heavy chain is structured into two domains. The head (globular) domain incorporates the ATP-sensitive track-interacting region and the ATP hydrolysis. The tail (extended) domain is responsible for linking motor to cargo by interacting with other subunits (Asai and Wilkes, 2004).

Motor proteins act as molecular machines that are capable of cell motility by utilizing energy derived through ATP hydrolysis. In cytoplasm, cellular cargos and vesicles are transported by driving force of motor proteins. Several motor proteins (kinesin and cytoplasmic dynein) play important role in intracellular transport (axonal transport), spindle apparatus formation and chromosomes separation during cell division process (Howard, 2001).

3D structure of *rattus norvegicus* Dynein light chain 8 in complex with BCL2-LIKE 11(Bim) peptide (PDB ID: 1F95) was retrieved through Protein Data Bank (Fan *et al.*, 2001). Reported binding motifs [(K/R)XTQT and G(I/V)QV(D/E)] (Puthalakath *et al.*, 1999; Lo *et al.*, 2001,

Rodriguez-Crespo *et al*., 2001) of Dynein light chain LC8 with Bim were isolated through extensive literature survey (Rapali *et al.*,2011). 3D structure of Bim (1-9 AA) was retrieved through PDB ID: 1F95. The amino acid sequences of Tctex1 (UniProtKB - P51807, 1-113 AA) and Tcte3 (UniProtKB -P119851, 191AA) were retrieved from UniProt Knowledgebase database (Boutet *et al.*, 2016) in FASTA format. Position-Specific Iterative Basic Local Alignment Search Tool (PSI-BLAST) (Altschul *et al.*, 1990) was used against Protein Data Bank (PDB) (Sussman *et al.*, 2008) for suitable template search. The crystal structure of *Drosophila* Dynein Light chain Tctex-1 (PDB ID: 1YGT) was used as template. Comparative modeling was employed to generate 3D structure of mouse Tctex1 and Tcte3 by MODELLER 9.13 (Eswar *et al.*, 2008).

In the absence of experimentally known structure, 3D structure prediction of protein from its amino acid sequence is the most important solution in computational structural biology. Under such conditions, comparative modeling is one of the most precised computational approaches to predict a consistent 3D structure from sequence information (Tramontano, 1998).

Due to lack of a well-defined or experimentally determined structure, protein 3D structures are predicted by homology modeling method. It is based on sequence alignment of query and target protein whose structure is experimentally resoluted (Rayan, 2009). MODELLER 9.13 (Webb and Sali, 2014) was used for homology modeling. It is a command-based tool which takes query protein sequence as input and generates an output

model for the target protein by including all non-hydrogen atoms. It employs a method known as satisfaction of spatial restraints motivated by NMR spectroscopy data processing. In MODELLER, a set of geometrical criteria is used to produce probability density functions (pdfs) for the location of each atom in the protein (Gibrat *et al*., 1996). Following five steps were involved in the model generation.

Amino acid sequences of query proteins were retrieved through UniProtKB (Uniprot Consortium, 2008).

Retrieved sequences were subjected to PSI-BLAST (Altschul *et al.*, 1997) search against Protein Data Bank (*http://www.rcsb.org*) (Berman *et al.*, 2006) for suitable template search. The template searching was performed by considering identity, E-value and query coverage.

Sequence alignment is the second step of homology modeling. In this step, query and template sequences are aligned. The significance of an alignment is usually determined by E- and p-values

of the resulted sequence alignment. *Align2d* command of MODELLER 9.13 was used to align the query and template sequences. *Align2d* implements global dynamic programming with an affine gap penalty function (Eswar *et al.,* 2008) and is preferred for aligning the sequences as it tends to place gaps in a better structural context (Shen and Sali, 2006).

For model evaluation, model quality and potential errors in 3D models were assessed through different web servers ProSa-web (Wiederstein and Sippl, 2007), ERRAT (Colovos, 1993), VERIFY 3D (Eisenberg *et al*., 1997), RAMPAGE (Lovell *et al.,* 2003) and MolProbity (Chen *et al.,* 2010).The recognized tool ProSA often used in refinement, validation of experimental protein structures and *in-silico* protein modeling by means of Z-score representation. The model quality evaluates through Z-score by comparing with known protein structures (Z-score).The evaluated Z-score must be within the range of value for similar size protein chains. ERRAT uses a novel method for differentiating between correctly and incorrectly determined regions of protein structures based on characteristic atomic interaction. ERRAT quadratic error function is used to characterize the set of pairwise interactions from nine-residue sliding windows in a database of 96 reliable protein structures (Colovos and Yeates, 1993). Verify 3D assigns a structural class on the basis of location and environment to determine the compatibility of 3D model with its own 1D primary sequence. RAMPAGE generated a Ramachandran plot and provides information about favored, allowed and outlier regions. The structure validation tool MolProbity evaluates proteins on both local and global level. MolProbity relies on power and sensitivity provided by optimized hydrogen placement and all-atom contact analysis, covalent-geometry and torsion-angle criteria (Chen *et al.,* 2010). Model refinement and geometry optimization was done by WinCoot (Emsley *et al*., 2010) and UCSF Chimera 1.8.WinCoot displays maps and models and allows model manipulations such as idealization, real space refinement, manual rotation/translation, rigid-body fitting, ligand search, solvation, mutations, rotamers, Ramachandran plots, skeletonization, and non-crystallographic symmetry (Lohkamp *et al*., 2005). UCSF Chimera 1.8 is an extremely extensible program for interactive visualization and analysis of molecular structures, including density maps, supra-molecular assemblies, sequence alignments, docking results, trajectories, energy minimization and conformational ensembles (Pettersen *et al*., 2004).

Multiple and pairwise sequence alignment was carried out for Tctex1 and Tcte3 with 1YGT and LC8. Multiple sequence alignment was done for Tctex1 and Tcte3 to inspect the sequence similarity of the proteins with selected template IYGT using CLC Main Workbench. Pairwise alignment for Tctex1 with LC8 and Tcte3 with LC8 was carried out using EMBOSS needle (Li *et al.,* 2015) to explore the similarity of the proteins at sequence level.

CLC Main Workbench is used by tens of thousands of researchers all over the world for DNA, RNA, and protein sequence data analysis (Workbench, 2010).

Emboss needle requires two input FASTA sequences and marks their optimal global sequence alignment to output file. It works on the Needleman-Wunsch alignment algorithm for obtaining optimum alignment (including gaps) of two sequences along their entire length. The algorithm uses a dynamic programming method by exploring all possible alignments to ensure the optimal alignment.

To obtain best native conformation and predict a reliable interaction, computational approach (Protein-Protein docking) was employed to examine the binding region of respective proteins (Tctex1 and Tcte3). The molecular docking was performed by using AutoDock tools 4 (Morris *et al*., 2009), AutoDock Vina (Trott and Olson, 2010), ClusPro (Kozakov *et al.,* 2013) and HADDOCK (de Vries and Bonvin, 2011) to identify binding grooves of Tctex1 and Tcte3 against Bim peptide (apoptotic facilitator) as well as for homodimerization.

AutoDock is a suite of automated docking tools. It is designed to predict how small molecules, such as substrates or drug candidates bind to a receptor of known 3D structures. Current AutoDock distribution comprises two generations of software (AutoDock4 and AutoDock Vina). AutoDock Vina significantly improves the average accuracy of the binding mode predictions compared to AutoDock4. In AutoDock4 and AutoDock Vina analysis, ligand and receptor molecules were prepared by assigning kollman charges and adding polar hydrogen atoms. The docking experiments were performed with a rigid receptor and flexible ligands by allowing all torsions to rotate. In AutoDock4, for each ligand 100 independent docking runs were carried out with a grid map and spacing in Angstroms (Å). The empirical free energy function and Lamarckian genetic algorithm (LGA) was applied with the following parameters: a population of 150, maximum number of 27,000 generations, a mutation rate of 0.02, crossover rate of 0.80 and

number of energy evaluations was 2.5 x 10^6. The remaining docking parameters were set to default. Subsequently, results were clustered according to RMSD criterion and the ideal docked conformations of ligands were selected on the basis of binding free energy values to evaluate Tctex1 and Tcte3 binding with Bim. The best docked complex for each ligand was selected and interactions were monitored using DIMPLOT (Wallace *et al.*, 1995) which generated a plot of interactions

HADDOCK is a popular docking program that takes a data-driven approach for docking, with support for a wide range of experimental data. HADDOCK is the combination of two computational approaches, interface prediction and docking to obtain atomic-level structures of protein-protein complexes. The HADDOCK server has access to the resources of a dedicated cluster and of the e-NMR GRID infrastructure. Therefore, a typical docking run takes only a few minutes to prepare and a few hours to complete (De Vries *et al.*, 2010). Interface prediction comprises a set of optimal restraints for data-driven docking using HADDOCK. The six interface prediction web servers are combined in a consensus method called CPORT (Consensus Prediction Of interface Residues in Transient complexes). CPORT predictions were used to dock the full protein-protein benchmark, excluding only antibody-antigens and multimer complexes, using HADDOCK. CPORT predictions were shown to be more reliable and resulted in at least an acceptable docking solution in the top 400 for the majority of the complexes (de Vries and Bonvin, 2011). In first step, tertiary structures of Tctex1,Tcte3 and Bim were submitted to CPORT server for prediction of interface residues (active and passive).These residues were utilized as input in HADDOCK. Similarly, in case of dimerization, two monomers of each protein were submitted to HADDOCK after CPORT. The top ranked clusters were selected for further experimentation.

ClusPro is a docking tool which rapidly filters the output from the Fourier correlation algorithm using a combination of desolvation and electrostatic energies (calculated using a Coulomb potential). This approach results in several near-native structures passing through the filter, while eliminating many of the false positives. To monitor the interaction, docking analysis was also performed through ClusPro (Kozakov *et al.*, 2013). ClusPro uses three main steps, a rigid body docking program (PIPER) based on novel Fast Fourier Transform (FFT) technique with pairwise potential. The 1000 suitable energy conformations are clustered and 30 largest clusters are

retained for refinement by detecting native and non-native clusters. The stability of clusters is analyzed by Monte Carlo simulations and refinement is performed by SDU (Semi-Definite programming based Underestimation). In ClusPro, input PDB files were of Tcte3, Tctex1 and Bim, which resulted in four predicted models (Balanced, Electrostatic-favored, Hydrophobic-favored and VdW+Elec). Models were ranked by cluster size and lowest binding energy values.

Molecular Dynamics (MD) simulation of suitable docked complexes was performed by GROMACS 5.7.4 version (Schumann-Gillett *et al.,* 2017). GROMACS is a high end, high performance research tool designed for the study of molecular dynamics. Best docked complexes Tctex1-Bim and Tcte3-Bim were subjected to GROMACS for molecular dynamics simulation analysis. A detailed analysis was performed to evaluate the conformational changes, folding, stability, and dynamic behavior of interacting proteins. All MD simulations were performed on highly efficient OpenSuse Linux system using Amber03 force field by GROMACS. MD simulation assay consists of three stages: First, preparation of simulation system. Second, the simulation run and third one the results have to be analyzed.

Before MD simulations, the complex was needed to be optimized. AutoDock4 was used to check any missing atom and to repair the missing atoms in the complex.

Since the structure of protein complex obtained through molecular docking only contains coordinates, there is a need to build the topology, which illustrates the system in terms of atom types, charges and bonds etc. This topology is specific to a certain force field. We used AMBER03 force field (Duan *et al.,* 2003), which fits the dihedral potentials to new structure and constructs the topology. The *pdb2gmx* command was used to build topology file for molecules consisting of distinct building blocks (amino acids). The topology file is very important as it contains all the force field parameters and the respective hydrogen atoms according to the chosen force field. AMBER03 force field and Tip4p water model was selected.

Before adding the solvent, a general layout (space/box) of the simulation setup had to be chosen. Most frequently, simulations are performed under periodic boundary conditions (PBC). A single unit cell is defined, which can be stacked in a space filing manner. In this way, an infinite periodic system can be simulated by avoiding edge effects due to walls of simulation volume.

There are only a few general shapes available to set up PBC. We selected the octahedron unit cell. To disallow direct interactions among periodic images, a minimal distance of 1.0 Å was set between protein and wall of cell (the two neighbors should not be closer than 2.0 nm). PBCs were set with *editconf* command. After the unit cell setup, solvent was added. There are several solvent models, each of which is more or less intimately linked to a force field. Amber03 force field is generally used with Tip4p water model.

After solvation, system contains charged proteins. Total charge on the system was calculated and system was neutralized by adding counter ions to solution.

After neutralization, next step was to minimize the energy of system to 500 steps through steepest descent algorithm, by a tolerance of 1000 kJ/molÅ$^{2.}$ PBCs were applied in all directions. Normally, the system needs to be minimized in order to remove any local strains. These strains are result of small errors in the original structure such as Vander Walls contacts. Even small differences between GROMACS force field to improve PDB structures lead to unrealistically high forces among atoms. By energy minimization (EM), clashes can be removed.

To evaluate the success of EM, two important factors are used. The first one is potential energy (indicated at the end of the EM process). The potential energy should be negative for an apo protein or protein complex in water. It depends on the system size and the number of water molecules. The second important attribute is the maximum force (Fmax), the target for which it is defined by minim.mdp- "emtol = 1000.0 (representing a target Fmax of no greater than 1000 kJ $mol^{-1}nm^{-1}$).

Following the minimization step, system was subjected to equilibration for 1000 ps under constant temperature (300 K). The pressure was set to 1 ATM in NVT (isothermal-isochoric, constant number of particles, volume, and temperature) and NPT (isothermal-isobaric) ensemble, with a time step of 2 fs for geometric integration with leap frog algorithm.

Finally, the system was ready to run simulations. MD runs for 20 ns time scale under constant temperature and pressure conditions were performed. Particle Mesh Ewald (PME) algorithm (Abraham and Gready, 2011) was used to calculate long range electrostatic interactions.

Trajectories were analyzed by using tools embedded in GROMACS package. Snapshots were collected throughout MD simulations of each system and PDBs were generated for 1, 5, 10, 11, 15, 18 ns intervals to investigate the time-dependent behavior and stability of each system. GROMACS and UCSF Chimera were used to analyze the stability and behavior of each system.

The 3D structures were validated through geometrical analysis. The analysis included rotamer evaluations, ramachandran plots and Cβ deviations. The overall geometry of models including residual distribution is represented in Table 3.2.

The sequence and structural comparison of target proteins with template was observed by multiple sequence alignment and structural superimposition (Figure 3.1). The multiple sequence alignment between Tctex1, Tcte3 and 1YGT revealed 80-100% conservation. TcTex1 and TcTe3 exhibited high structural conservation with *Drosophila* Dynein Light chain Tctex-1. The superimposition of template and target proteins was based on their C-alpha or backbone atoms. The superimposed structures (1YGT-Tctex1 and 1YGT-Tcte3) exhibited RMSD values of 0.316Å and 1.167Å, respectively. Energy minimization was applied on the predicted models to improve their stereochemistry and to remove the energy constraints. The stereochemistry of Tctex1 and Tcte3 significantly was improved. The minimization was performed using ff99SB forcefield with AMBER parameters. The predicted 3D models for TcTex1 and TcTe3 were validated through different evaluation tools.

Due to absence of experimentally known structures, a comparative modeling technique was utilized to predict 3-dimensional structures of mouse Tcte3 and Tctex1.The retrieved amino acid sequences of Tctex1 and Tcte3 were subjected to PSI-BLAST for suitable template search. The crystal structure of *Drosophila* Dynein Light chainTctex-1(PDB ID: 1YGT) was selected as an appropriate template on the basis of sequence identity and query coverage with target sequences (

The overall model quality was assessed by Z-score. The calculated Z-score value measures the energy divergence of structure against energy distribution resulting from random conformations. The Z-scores for predicted Tctex1 and Tcte3 models determined the separation between native folds and misfold assembly on the basis of standard deviation unit assembly. The calculated Z-scores for Tctex1 (-5.28) and Tcte3 (-3.47) validated the abilities of knowledge-based potentials. The Z-score was calculated to identify the native folds. The 3D predicted models for Tctex1 and Tcte3 were subjected to ERRAT protein structure verification server. A 9-residue sliding

window used quadratic error function to distinguish the pairwise interactions. ERRAT provided overall quality factor for both models was greater than 70%. The ERRAT values differentiated the correct and incorrect regions of protein structures on the basis of atomic interactions.

The RAMPAGE gave results in the form of Ramachandran plots. Ramachandran plot exhibits the residual and phi (Φ)and psi (Ψ) angle distribution against non-Proline and non-Glycine residues. The phi and psi angles were used to assess the distinction of favored and unfavored regions. In Ramachandran analysis, 99% and 85% residues of Tctex1 and Tcte3 were lying in most favored regions, respectively.

Dynein light chains (LC8, Tctex1 and Tcte3) were compared at sequence and structure level to elucidate the similarities among LC8, Tctex1 and Tcte3 which might be useful to deduce functional relevance. The pairwise sequence alignment was used to compare primary sequences of dynein light chains (Tctex1, Tcte3 and LC8). The superimposition of 3D structures of focused dynein light chain complexes (LC8-Tctex1 and LC8-Tcte3) was performed to infer suitable structural and functional conservation of Tctex1, Tcte3 with LC8. This analysis suggested that LC8-Tctex1 was more conserved than LC8-Tcte3 at sequence level. However, LC8, Tctex1 and Tcte3 light chains were more conserved at structural level than sequence. The LC8-Tctex1 pairwise sequence alignment exhibited an alignment score of 15.5%, while superimposition of LC8 and Tctex1 yielded an RMSD value of 1.412Å. In case of LC8-Tcte3 superimposition, the RMSD value (0.953Å) was considered more reliable for Tcte3 structural similarity with LC8 than

Tctex1. The pairwise sequence alignment of LC8 and Tcte3 revealed an alignment score of 13.0%. Tctex1 and Tcte3 exhibited elongated β-sheets as compared to LC8. Dynein light chain LC8 consists of two α-helices and four β-sheets named as β1, β2, β3 and β4 (Figure 3.2). The Tctex1 and Tcte3 followed the same topology as LC8 with differences in the number of β-sheets. Hence, structural comparison is a clear approach to deduce the functional propensities of light chains.

The critical regulatory role of LC8 in a variety of systems is due to its capability to endorse dimerization of chaotic proteins (Barbar, 2008). The crystallographic and NMR studies exposed that Bim, nNOS and Swallow bind to LC8 dimer in the vicinity of binding grooves. The past studies revealed binding at dimer interface (Fan *et al., 2001* and Benison *et al.,* 2007). LC8 acts as a dimerization engine in dynein (Makokha *et al.,* 2002). In the reported LC8-Bim RAT dynein

motor complex (PDB ID: 1F95), LC8 dimer conformation contains two pairs of α-helices covering in opposite faces, and each pair of helices packs against a β-sheet with 5 antiparallel β-strands. Each 5-stranded β-sheet exhibits 4 strands from one monomer and a 5th strand from the other monomer. A 13-residue peptide from nNOS is bound to the dimer in the deep hydrophobic groove as a 6th antiparallel β-strand (Liang *et al.,* 1999). LC8 exists as a homodimer both in the absence and presence of its target proteins. LC8 dimer displays a rectangular symmetry due to extensive hydrogen bonds and hydrophobic interactions of both monomers.

To elucidate the dimer orientation of mouse Tcte3 and Tctex1, their models were subjected to docking analysis. The resulted dimers adopted similar orientation as reported structures of LC8 (PDB ID : 1F95; Fan *et al.,* 2001) and human LC8-Bim complex (PDB ID: 1CMI; Liang *et al.,* 1999). In rat LC8 dimer (1F95), β2-strand of one monomer was linked with β2-strand of other monomer through hydrogen bonding. Gly63 and Cys56 residues of one monomer were involved in hydrogen bonding with Val58 and Tyr65 of second monomer (Figure 3.3). The conformational topology of crystallographic structure (LC8-Bim) complex exhibited two grooves at opposite sides of dimer interface.

In Tctex1 dimer, the binding groove at dimer interface was similar to LC8 and Tcte3 (Figure 3.4). The investigation of Tctex1 dimer interface exhibited uniform pattern of interaction between both monomers. Consequently, from one monomer Ser107, Ser88 and Asp86 residues were implicated in hydrogen bonding with His78, Asn73 and Gln71 residues of the other monomer. Hence, residues of one monomer were located at β-strands and loop region, which manifested the interactions with residues at β-strand and loop region of other monomer. In case of Tctex1 dimer interaction with Bim some conserved residues (Ser81, Ser82, Cys83, Phe84 and Trp85) was observed.

The Tcte3 dimer form exhibited 4 β-sheets (Figure 3.5). β2-strand was converted into loop region, which was engaged in dimerization. The residues of one monomer (Asp124, Phe140, Ile142 and Gln152) were involved in hydrogen bonding with second monomer residues (Ala157,

Arg159, Gln143 and Asp113). In Tcte3 dimer few conserved residues (Asn155, Ile156, Ser158, Trp160 and Asp163) which involved in binding with Bim to form ternary complex.

In current study, our goal is to investigate the binding grooves of Tctex1 and Tcte3. The docking analysis of Tctex1 and Tcte3 dimers against pro-apoptotic facilitator (Bim peptide) was performed. The analysis was investigated the binding grooves of Tctex1, Tcte3 for Bim peptide and homodimerization (Figure 3.6 and 3.7). We mapped binding of Bim with dimer form of Tctex1 and Tcte3 to monitor their binding grooves. We encapsulated the major interactions between Tctex1, Tcte3 and Bim peptide. The target Bim peptide accomplished the formation of antiparallel β-strand to the pre-existing β-sheets of Tctex1 and Tcte3, resulting in a tetrameric complex (Figure 3.4 and 3.5). These results were remarkably firm with the previously known ternary complex of LC8-Bim dimer. The analysis revealed that dimerization interface and Bim peptide binding groove attain similar topology in dynein light chains.

In order to characterize the binding of Bim with Tcte3 and Tctex1, initially, we evaluated known apoptotic complex of LC8 and Bim (Rapali *et al*., 2011) via docking analysis. These observations led us in establishing training data set and docking protocol for comparative docking analysis of Tctex1 and Tcte3 with apoptotic factor Bim (Figure 3.8). The findings were ranked on the basis of lowest energy values (Tables 3.3 and 3.4) for detailed analysis.

The detailed binding residues of individual apoptotic factor (Bim) with Tctex1 and Tcte3 were depicted in Tables 3.4 and 3.5. LC8 conserved residues (Thr70, Glu69, Val66, His68, Ser64, Phe62 and Tyr77) lie at β2-L4-β3 region are involved in interactions with Bim (Fan *et al.,* 2001). In case of Tcte3 and Tctex1, binding of Bim peptide was detected at the similar regions in Tcte3 and Tctex1. Tctex1 specific Ser81, Ser-82, Cys-83, Phe-84, Trp-85, Ser-92, Arg-96 and Ser87 residues were involved in binding with Bim (Figure 3.8A), while binding region of Tcte3 was comprised of Asn155, Ile156, Trp160, Asp167, Trp169, Lys87, Ile161, Trp162, Asp163 and Trp166 residues (Figure 3.8B).

Elucidation of conformational changes, stability and dynamic behavior of respective protein complexes (TcTe3-Bim and TcTex1-Bim) were observed by MD simulation assays. Consequent trajectories were meticulously analyzed to estimate constancy, junctions, vigorous, functional and structural characteristics while running simulations.

Time succession of root mean square deviation (RMSD), root mean square fluctuation (RMSF) were evaluated to predict the stability and fluctuations of C-alpha atoms in bound and Apo forms. The overall stability of each complex was deliberated by calculating the RMSD profile (Figures 3.9 and 3.10). RMSD for each complex was intended by means of apo-form as a reference. The average RMSD values of respective protein complexes TcTe3-Bim with apo-Tcte3 (1.114 Å) (Figure 3.9A) and TcTex1-Bim with apo-TcTex1 (1.20 Å) (Figure 3.10A) represented a stable environment of systems.

RMSF values calculate the degree of residual fluctuations, which were reprsented by peak altitude in graphs (Figures 3.9B and 3.10B). In TcTex1-Bim complex, major fluctuations were present in residues namely Gln35 (0.1728 Å), His36 (0.1848 Å), Lys72 - His78 (0.1824-0.3403 Å) and Thr101 (0.1626 Å) (Figure 3.9B). These fluctuations were located in the loop regions except His-36 that fluctuated in α1 (Figure 3.9B). However, interacting residues involved in binding with Bim peptide (Lys62, Ile64, Thr66, Val68, Ile69, Met70, Gln71, Leu77, Ser79, Ala80, Ser81, Ser82, Cys83, Phe84, Ile105, Ser107, Phe109 and Leu111) were stable except Leu-77. The Leu77 was fluctuated in loop4 region and it was considered as less stable. TcTex1 conserved residues (Ser81, Ser82, Cys83, Phe84, Trp85, Ser92, Cys93, and Arg96) involved in interaction with Bim located in the vicinity of binding region were observed more stable.

In Tcte3-Bim complex, key fluctuations were pragmatic in Asp-108 (0.3071 Å), Gln152-Ile154 (0.5428-0.5406 Å), Asp167 (0.3076 Å) and Ser178 (0.2624 Å) residues (Figure 3.8B). The TcTe3 residues (Lys87, Leu145, Phe146, Ile147, Ile154, Asn155, Ile156, Ser158, Trp160, Ile161, Trp162, Asp163, Trp166, Asp167, Trp169, Leu182 and Phe186) involved in Bim interaction revealed lesser fluctuations. These lesser fluctuations manifested more stability with a marked task in interaction. All conserved residues of TcTe3 (Leu87, Asn155, Ile156, Trp160 and Trp169) involved in interaction with Bim were stable, except Asp167 (0.3076Å). RMSF plot for Tcte3 indicated residual fluctuations in the loop regions, while comparatively no fluctuation was observed in the β-sheets and α-helical regions of Tcte3. Major fluctuations were observed in the loop regions of Tcte3 and Tctex1 (Figures 3.9 and 3.10).

In comparative structural analysis between apo-Tctex1 and Tctex1-Bim at 18ns, major conformational changes were considered as extension of apo-Tctex1 loop2 region (Gly30- Gln-35) to three residues (Gly30-Lys38) (Figure 3.11). The α2 region (His36- Leu54) of apo-Tcte3 shifted to residual range (Val39- Lys56) in Tctex1-Bim. In case of Tcte3-Bim complex, main changes were following: apo-Tcte3 loop1 region (Leu86-Ala91) extended to Leu86-Thr96. The α1 (His92-Ser105) in apo-Tcte3 drifted towards the α1 (Lys97-Asp108) with respect to Tcte3-Bim complex (Figure 3.12). Loop2 (Val109- Lys110) was shrinked with respect to apo-Tcte3 loop2 (Leu106- Lys114). The α2 (Ala115- Glu132) in free state of Tcte3 shifted by 4 residues with reference to Tcte3-Bim α2 (Tyr111-Val130). β1 (Lys139-Val144) was shifted to Phe140-Gln148 as compared to apo-Tcte3.

Cell apoptosis is a complicated process which is influenced by various biochemical factors such as hormone level and pathway-specific apoptotic factors (Chausiaux *et al.,* 2008; Ruwanpura *et al.,* 2008). Cell death plays an essential function in multicellular organisms throughout their early development in sculpting the body organs by scheming cell homeostasis (Saikummar *et al.,* 1999). Apoptosis protects the organism by eliminating the cells injured by disease, infection, genetic mutation, aging and exposure to toxic agents (Wyllie *et al.,* 1980). Apoptosis has been recognized as a main feature that contributes to male infertility as it is necessary for usual spermatogenesis in mammals. A sufficient amount of germ cells is removed through apoptosis to maintain a particular germ cell population (Vaithinathan *et al.,* 2012).

Tctex1 (Tctex1 domain containing 1) and Tctex2/Tcte3 (t-complex-associated testis expressed 3) are germ cell-specific proteins that are expressed in testis and sperm. These proteins play an important role in male germ cell development (Ha *et al.,*1991; Huw *et al.,* 1995; Harrison *et al.,* 1998). Tcte3 and Tctex1 proteins exhibit high structural similarity to LC8 (PDB ID: 1F95). The LC8 monomer subunit comprises a small N-terminal strand followed by two helices (*α*1, *α*2). These helices are jam-packed against a 5-stranded β-sheetformed by one N-terminal strand and 4 other strands, one of which is consequent from the neighboring monomer. Two well-organized monomers form a symmetrical dimer (Kausar *et al.,*2013).We observed that Tctex1,Tcte3 and

LC8 are structurally more conserved than at sequential level. Tctex1 and Tcte3 have the same structural topology as LC8 except the differences in β-sheets. The Tctex1 and Tcte3 β-sheets were more extended than that of LC8 β-sheets. Possibly, Tctex1 and Tcte3 may exist in dimer form in a similar way to that of LC8.The two LC8 monomers form a dimer through interactions between β2-strands of both monomers (Fan *et al.,* 2001). We elucidated the dimer formation of Tctex1 and Tcte3 by docking analysis. In both cases, the orientation was similar to LC8 dimer. It was demonstrated that homodimerization of all three dynein light chains (LC8, Tctex1 and Tcte3) resulted the two binding grooves at dimer interface where ligands can accommodate, while overall topology of homodimers was preserved in all three proteins. We scrutinized the dimerization interface by the association of Bim (BH3-only protein) peptide at the binding groove. LC8 interacts with multiple viral and cellular proteins through its small consensus motif (K/R)XTQT.In LC8 targeted proteins, presence of two conserved consensus sequence motifs (K/R)XTQT and G(I/V)QV(D/E) is evident (Jaffrey and Snyder, 1996; Rodriguez-Crespo *et al.,* 2001; Lo *et al.,* 2001).

Tcte3 and Tctex1 are known to interact with LC8 and its target proteins (Lo *et al.,* 2001; Williams *et al.,* 2005; Mok *et al.,* 2001). Among them, a pro-apoptotic protein Bim has been reported to interact with LC8 that contains only 9 residues (MSCD**KSTQT**) (Puthalakath *et al.,* 1999; Fan *et al.,*2001). LC8 binding groove for Bim involves β2-L4-β3 region. The Bim binding groove is generated between the two monomers by incorporating β1, β3and mainly loop region which is evolved from β2-strand of LC8. Due to high structural similarity in Tctex1, Tcte3 and LC8, it was observed that through dimerization,Tctex1 and Tcte3 formed a similar groove to that of LC8 for binding to Bim. Predominantly, hydrophobic residues of loop and β-strand regions were involved in the formation of hydrophobic surface for Bim binding. We also performed molecular dynamics of apo-Tctex1, apo-Tcte3 and their complexes with Bim. The analysis indicated an overall stable binding profile for all systems which suggested that interactions of Tctex1 and Tcte3 with Bim were present in the vicinity of binding grooves.

Recent studies argue the role of Dynein light chains (DLCs) in apoptotic induction by linking the compartmentalization of pro-apoptotic cargoes (Puthalakath *et al.,*2004; Izidoro-Toledo *et al.,*2013). It is a well-knownfact that sequestering of Bcl-2 family proapoptotic protein Bim to microtubule-associated dynein motor complex is mediated by LC8 (Puthalakath *et al.,* 1999).

Upon apoptotic stimuli, LC8 binding with dynein motor complex is disrupted and free LC8 interacts with Bim to neutralize the anti-apoptotic activity of Bcl-2.

Under normal conditions, LC8-Bim complex sequesters Bim to the microtubule-associated dynein complex. Upon apoptotic stimulation, LC8-Bim complex is released from the microtubule resulting in the dissociation of Bimthat is free to neutralize the anti-apoptotic activity of Bcl-2 by forming a Bim/Bcl-2 heterodimer (Puthalakath *et al.*,1999). It has been demonstrated that MEFs (mouse embryonic fibroblasts) lacking Bim/Bmf or Bax/Bak complexes are less susceptible to cell death than wild-type MEFs, suggesting the requirement of pro-apoptotic proteins as mediators of intrinsic apoptotic pathway in the absence of caspases (Gavathiotis *et al.*,2008). Tctex1 and Tcte3 may transduce apoptotic signals to mitochondria by interacting with Bim in a similar manner to that of LC8 (Luo *et al.*, 2013). Phosphorylation of Bim by Pak1 (p21-activated kinase-1) may result in their dissociation from Tctex-1 family (Tctex1 and Tcte3)and subsequent degradation by ubiquitin-proteasome. In the absence of free Bim, MAPK8/JNK (Mitogen-Activated protein kinase-8/c-Jun N-terminal kinase) is unable to phosphorylate and inhibit downstream signaling events to neutralize the anti-apoptotic Bcl-2 protein in mitochondria thus promoting cell survival.In response to apoptotic stimuli, Bim dissociates from Tctex-1 family and free apoptotic proteins are phosphorylated by JNK/MAPK8. Through phosphorylation, stable Bimtranslocates to the mitochondria and activates other apoptotic facilitators like Bax, Bad and Bak to neutralize the effect of anti-apoptotic proteins like Bcl-2 and promote release of cytochrome-c thereby triggering the apoptosis via mitochondria-mediated pathway.

Conclusively, our detailed analysis investigated the sequence and structural similarities with LC8. We analyzed homodimerization of Tctex1 and Tcte3 by identifying binding grooves that might play an important role in interaction with Bim pro-apoptotic facilitator. We proposed common binding partner Bim for Tctex1 and Tcte3 which is involved in apoptosis by exploring similar mode of interaction to LC8. Our *in-silico* analysis explored the role of Tctex1 and Tcte3 in apoptosis on the basis of structural similarity and functional relevance with LC8.

In future, we aim to perform further computational approaches to investigate binding of dynein light chains Tctex1 and Tcte3 with Bim and dynein intermediate chains to explore the role of whole dynein complex In apoptotic pathway.

thesis

ORIGINALITY REPORT

%12	%9	%9	%
SIMILARITY INDEX	INTERNET SOURCES	PUBLICATIONS	STUDENT PAPERS

PRIMARY SOURCES

1	lib.bioinfo.pl Internet Source	%1
2	www.jove.com Internet Source	<%1
3	secure.hosting.vt.edu Internet Source	<%1
4	fusion.bu.edu Internet Source	<%1
5	www.linknovate.com Internet Source	<%1
6	Hódi, Zsuzsa, Attila L. Németh, László Radnai, Csaba Hetényi, Katalin Schlett, Andrea Bodor, András Perczel, and László Nyitray. "Alternatively Spliced Exon B of Myosin Va Is Essential for Binding the Tail-Associated Light Chain Shared by Dynein†", Biochemistry, 2006. Publication	<%1
7	emboss.open-bio.org Internet Source	<%1

8	saturn.roswellpark.org Internet Source	<%1
9	www.mdpi.com Internet Source	<%1
10	Hirokawa, N.. "Molecular Motors in Neurons: Transport Mechanisms and Roles in Brain Function, Development, and Disease", Neuron, 20101118 Publication	<%1
11	migale.jouy.inra.fr Internet Source	<%1
12	www.ncbi.nlm.nih.gov Internet Source	<%1
13	www.scc.acad.bg Internet Source	<%1
14	linknovate.com Internet Source	<%1
15	www.reproduction-online.org Internet Source	<%1
16	www.qiagenbioinformatics.com Internet Source	<%1
17	Izidoro-Toledo, T C, A C Borges, D D Araújo, D P S Leitão Mazzi, F O Nascimento, J F Sousa, C P Alves, A P B Paiva, D M Trindade, E V	<%1

Patussi, P M Peixoto, K W Kinnally, and E M Espreafico. "A myosin-Va tail fragment sequesters dynein light chains leading to apoptosis in melanoma cells", Cell Death and Disease, 2013.
Publication

18	www.structuralbiology.eu Internet Source	<%1
19	eprints.utm.my Internet Source	<%1
20	discovery.org.in Internet Source	<%1
21	A Vazquez. "TGFβ-mediated apoptosis of Burkitt's lymphoma BL41 cells is associated with the relocation of mitochondrial BimEL", Oncogene, 05/29/2008 Publication	<%1
22	synaptica.es Internet Source	<%1
23	Amit Kumar Banerjee. "Aspartate carbamoyltransferase of Plasmodium falciparum as a potential drug target for designing anti-malarial chemotherapeutic agents", Medicinal Chemistry Research, 08/17/2011 Publication	<%1

24	Dima Kozakov. "Achieving reliability and high accuracy in automated protein docking: ClusPro, PIPER, SDU, and stability analysis in CAPRI rounds 13-19", Proteins Structure Function and Bioinformatics, 2010 Publication	<%1
25	Maria E. Ariza. "Cell Cycle and Apoptosis", Environmental Metal Pollutants Reactive Oxygen Intermediaries and Genotoxicity, 1999 Publication	<%1
26	K. Döhner. "The Role of the Cytoskeleton During Viral Infection", Current Topics in Microbiology and Immunology, 2005 Publication	<%1
27	shodhganga.inflibnet.ac.in Internet Source	<%1
28	Satoshi Watanabe, Manami Harayama, Shingo Kanemura, Roberto Sitia, Kenji Inaba. "Structural basis of pH-dependent client binding by ERp44, a key regulator of protein secretion at the ER–Golgi interface", Proceedings of the National Academy of Sciences, 2017 Publication	<%1
29	Dehury, Budheswar, Jitendra Maharana, Bikash Ranjan Sahoo, Jagajjit Sahu, Priyabrata Sen, Mahendra Kumar Modi, and Madhumita	<%1

Barooah. "Molecular recognition of avirulence protein (avrxa5) by eukaryotic transcription factor xa5 of rice (Oryza sativa L.): Insights from molecular dynamics simulations", Journal of Molecular Graphics and Modelling, 2015.
Publication

30	www.breast-cancer-research.com Internet Source	<%1
31	www.researchgate.net Internet Source	<%1
32	Zhu, Jie, Min Wu, and Aruna Kalyanasundaram. "Structural and biomechanical basis of mitochondrial movement in eukaryotic cells", International Journal of Nanomedicine, 2013. Publication	<%1
33	Rajagopalan, Vidyalakshmi, Jonathan P. D'Amico, and David E. Wilkes. "Cytoplasmic dynein-2: from molecules to human diseases", Frontiers in Biology, 2013. Publication	<%1
34	springerplus.springeropen.com Internet Source	<%1
35	dmd.aspetjournals.org Internet Source	<%1

exp-oncology.com.ua

36	Internet Source	<%1
37	Newton, Kim, and Domagoj Vucic. "Ubiquitin Ligases in Cancer: Ushers for Degradation", Cancer Investigation, 2007. Publication	<%1
38	ir.stonybrook.edu Internet Source	<%1
39	Clementi, Nicola, Nicasio Mancini, Matteo Castelli, Massimo Clementi, and Roberto Burioni. "Characterization of epitopes recognized by monoclonal antibodies: experimental approaches supported by freely accessible bioinformatic tools", Drug Discovery Today, 2012. Publication	<%1
40	discovery.ucl.ac.uk Internet Source	<%1
41	Molitor, Christian, Stephan Gerhard Mauracher, and Annette Rompel. "Aurone synthase is a catechol oxidase with hydroxylase activity and provides insights into the mechanism of plant polyphenol oxidases", Proceedings of the National Academy of Sciences, 2016. Publication	<%1
42	Lu, S.Y.. "Molecular docking and molecular	

	dynamics simulation studies of GPR40 receptoragonist interactions", Journal of Molecular Graphics and Modelling, 201006 Publication	<%1
43	Madhu Sudhana Saddala, A. Usha Rani. "Chapter 7 Homology Modelling, Structure-Based Pharmacophore Modelling, High-Throughput Virtual Screening and Docking Studies of L-Type Calcium Channel for Cadmium Toxicity", Springer Nature, 2017 Publication	<%1
44	www.scribd.com Internet Source	<%1
45	Midoro-Horiuti, T.. "Major linear IgE epitopes of mountain cedar pollen allergen Jun a 1 map to the pectate lyase catalytic site", Molecular Immunology, 200312 Publication	<%1
46	Welte, M. A., and S. P. Gross. "Molecular motors: A traffic cop within?", HFSP Journal, 2008. Publication	<%1
47	Vallee, R.B.. "Autoinhibitory and other autoregulatory elements within the dynein motor domain", Journal of Structural Biology, 200610 Publication	<%1

48	Murrell, R. N., and J. E. Gibson. "Brevetoxin 2 alters expression of apoptotic, DNA damage, and cytokine genes in Jurkat cells", Human & Experimental Toxicology, 2011. Publication	<%1
49	M. Chaitanya. "Exploring the molecular basis for selective binding of Mycobacterium tuberculosis Asp kinase toward its natural substrates and feedback inhibitors: A docking and molecular dynamics study", Journal of Molecular Modeling, 02/07/2010 Publication	<%1
50	Forro, Gabriella(Daniel, P., Leutz, A. and Lipp, M.). "The signalling pathway of Bim L and Bim S, two isoforms of the BH3-only protein Bim, in apoptosis", Mathematisch-Naturwissenschaftliche Fakultät I, 2010. Publication	<%1
51	Chipuk, J.E.. "How do BCL-2 proteins induce mitochondrial outer membrane permeabilization?", Trends in Cell Biology, 200804 Publication	<%1
52	J. M. Adams. "The Bcl-2 Protein Family: Arbiters of Cell Survival", Science, 08/28/1998 Publication	<%1

EXCLUDE QUOTES	ON	EXCLUDE MATCHES	< 4 WORDS
EXCLUDE BIBLIOGRAPHY	OFF		